JOURNAL OF ULTRASTRUCTURE RESEARCH 92, 1–27 (1985)

Deep-Etch Views of Clathrin Assemblies

J. HEUSER* AND T. KIRCHHAUSEN†

*Department of Cell Biology and Physiology, Washington University School of Medicine, 660 South Euclid Avenue, St. Louis, Missouri 63110; and
†Department of Anatomy, Harvard Medical School, 25 Shattuck Street, Boston, Massachusetts 02115

Received April 22, 1985

Clathrin assemblies were adsorbed to mica and freeze-dried by a new procedure that yields 3-D images with much topological detail. These permitted renewed inquiry into how clathrin trimers (i.e., "triskelions") assemble into polygonal coats or baskets. Freeze-drying revealed unsuspected differences in the relative shapes and dimensions of individual trimer building blocks, as compared with the completed polygonal networks, which indicate that the assembly scheme first proposed by Crowther and Pearse (1) requires modification. Specifically, the freeze-etch images display the following new features: (1) Trimer arms possess terminal scroll-shaped hooks that can open or close and thus determine their lengths. (2) When extended, trimer arms are sufficiently long to pass around three sides of the final polygonal facet. Since current views hold that the arms pass around only two sides, the remaining length, including the terminal hook, must point into the basket interior. (3) Freeze-dried trimers display bends in their arms at specific loci that determine their final distribution in the completed baskets. (4) The completed struts of the final assemblies are uniform in calibre, cylindrical in profile, and travel directly between the vertices of each polygon, without any sign of the slew or width-variation that is predicted by the Crowther and Pearse model. Based on this direct comparison of protomer vs product, by a single technique that can image both, we offer a modified scheme for clathrin coat assembly, in which we predict that the individual arms in each clathrin triskelion emanate from its center in a slewed manner, but the final assembled struts of the basket need not be slewed. Attempts were made to capture assembly intermediates on mica to obtain support for the new scheme, but these unfortunately yielded ambiguous images of incomplete polygons with blunt projections, rather than the expected "halo" of uncommitted trimer arms. These we interpret to be "dead ends" that failed to polymerize further because they included proteolyzed components. Further assembly experiments, avoiding such hazards, are indicated.

In eukaryotic cells, budding or newly formed membrane vesicles are commonly surrounded by a polygonal lattice known as a clathrin coat or basket [reviewed in (3, 4, 7, 10, 21, 27)]. When such coated vesicles are isolated and their baskets depolymerized, they prove to be assembled from trimeric proteins which have a distinct pinwheel ("triskelion") shape (1, 12, 26). Each triskelion dissociates in SDS into three 180-kDa polypeptides termed heavy chains and three smaller species termed light chains (12, 19–21, 26). A major challenge is to understand how these polypeptides assemble into triskelions, how the triskelions assemble into polygonal lattices, and how the lattices come to associate *in vivo* with particular classes of budding membranes.

This paper analyzes the structure of clathrin trimers and polymers using the quick-freeze, deep-etch technique. Our images indicate that each arm of the trimer is hooked at the end and measures 52 nm *in toto,* substantially longer than previous measurements made of air dried triskelions where the hook is not visible (12, 14, 24, 26, 31). On the other hand, the struts that form the polygons of the completed basket measure 15.5 nm in comparable freeze-etchings. This is substantially shorter than previous measurements of negatively stained samples (1), which we show here are distorted. Taken together, these data indicate that each arm of the clathrin trimer can extend along two struts, as current models propose (1, 4, 27), and still have a substantial distal portion

0022-5320/85 $3.00

left over, which we propose can point inward to make contact with the membrane vesicle inside. In support of this, our images of freeze-fractured coated vesicles demonstrate that only a small proportion of the largest ones actually contain membrane vesicles; the rest contain internal "nuggets" of protein, which appear to include internally directed distal portions of trimer arms. Freeze-fractured baskets reassembled from pure clathrin display this internally directed material as well, whereas it is absent from baskets in which the terminal domains of trimers have been "clipped" by proteolysis. Finally, images of depolymerizing and repolymerizing baskets provide intriguing but ultimately inconclusive data on exactly how the polygons are assembled from triskelions. Nevertheless, a modified scheme for clathrin coat assembly is offered based on the new insights obtained in this study.

METHODS

Coated vesicles were isolated from calf brains as detailed in Ref. (13) and purified by D_2O/Ficoll isopycnic centrifugation (21). Clathrin was purified from brain coated-vesicle preparations by urea extraction and gel chromatography as detailed in Ref. (13). Baskets were repolymerized from purified clathrin by dialysis against the appropriate solutions (17, 22, 30, 32). Baskets were "clipped" by treatment with proteases as detailed in Ref. (14).

Samples were adsorbed to mica flakes in preparation for freeze etching in the manner described in Ref. (8). In brief, this involves grinding thin mica sheets into a fine powder and washing the powder briefly with 1 *M* KCl to render it hydrophilic. Mica flakes that remain in suspension at 1 *g* are collected in a clinical centrifuge, washed twice in 70 m*M* KCl, and spread as a thick paste on a slab of aldehyde-fixed rabbit lung. An aqueous suspension of the sample (15 μl at $\sim/\mu M$ concentration) is then placed on the mica and allowed to stand for 30 sec. Excess sample is then drawn off the mica paste and the whole sandwich is quickly plunged onto a liquid helium-cooled copper block (using a new "Cryopress" manufactured by Med-Vac, Inc., St. Louis, Mo.). The quick-frozen sample is then freeze fractured with a standard Balzer's cryomicrotome and etched *in vacuo* for 3 min at −100°C before being rotary replicated with platinum evaporated from an electron-beam gun mounted 10° above horizontal. The replica is next floated off the mica paste onto concentrated hydrofluoric acid and left overnight to remove any adherent mica. (Platinum-coated mica flakes stubbornly cling to the replica and must be completely dissolved.) The replica is then cleaned of organic materials with household bleach and mounted on Formvar-covered 400 mesh "Gilder" grids.

In the electron microscope, all fields are photographed in stereo at ±10° tilt and the resulting negatives are mounted in a Wild APT-1 stereo map reader which is interfaced (via camera lucida) to a Zeiss MOP-3 digitizing tablet and calculator. This permits simultaneous 3-D viewing and superimposed movement of a measuring stylus over the field, thus facilitating subjective discernment of optimal molecules for quantitation. Final plates are produced in reverse contrast by generating an internegative (the original EM negative contact printed onto another piece of Kodak EM 4489 film) and then printing from the internegative.

Magnification of the electron microscope is calibrated frequently with platinum replicas of molluscan hemocyanin molecules that have a distinct 10 nm helix on their surface (8). In critical instances, hemocyanin is mixed with the experimental sample before adsorption to mica, then mounted and freeze etched along with it, thus producing an internal standard in the same replica that will be measured.

RESULTS

1. *Clockwide and Counterclockwise Orientation of Clathrin Trimers*

In a separate publication (15), we report that clathrin trimers assume two different orientations depending on the ionic conditions existing during adsorption to a substrate. Here we describe how this phenomenon reflects specifically upon the technique of mica adsorption used as the first step in our quick-freeze, deep-etch technique (8).

Figure 1 shows brain coated vesicles destabilized with Tris buffer in the standard way (11, 26, 27, 30, 32) before exposure to mica. At Tris concentrations between 10 and 100 m*M*, virtually all of the clathrin trimers released by such destabilization attach to mica in a compact, symmetrical, clockwise configuration first seen by Ungewickell and Branton, a configuration that led them to the term "triskelion" (26, 27). Stereo views (Figs. 2, 3) illustrate that the vertices of such freeze-dried triskelions are elevated, hence coated with extra platinum. As we discuss elsewhere (15), this presumably reflects a preexisting "pucker" in the molecule while in suspension. This pucker

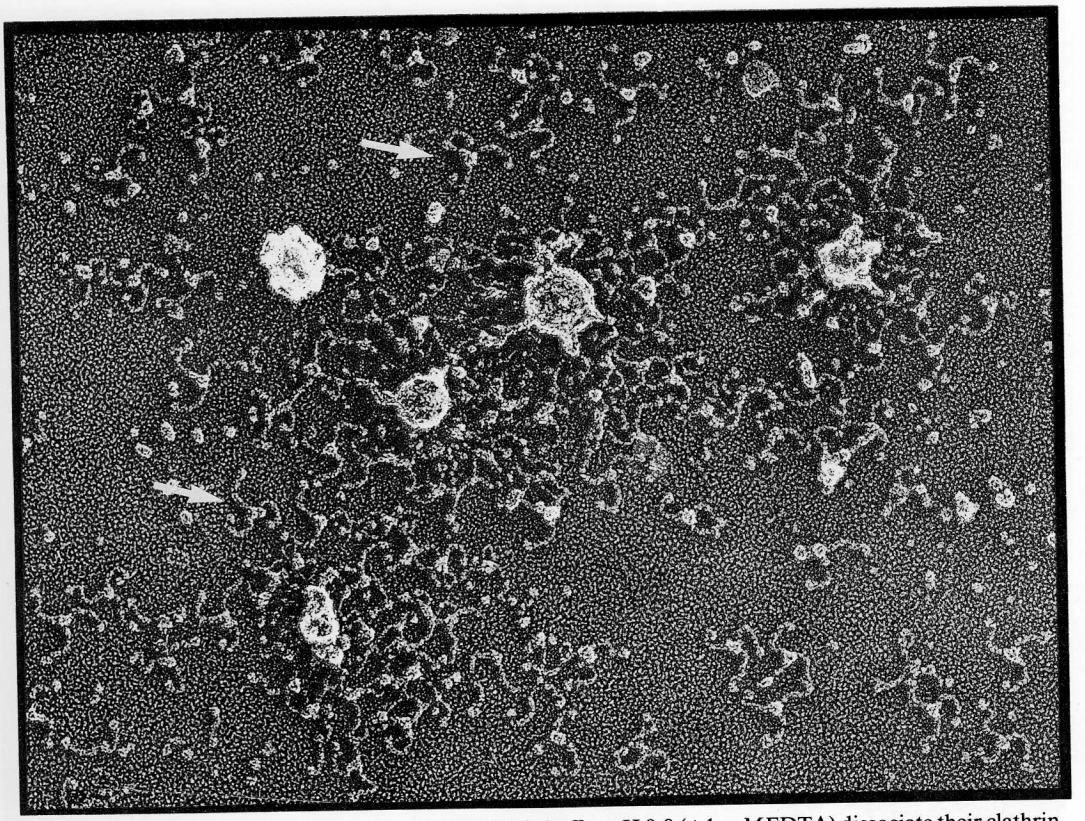

FIG. 1. Brain-coated vesicles exposed to 100 m*M* Tris buffer, pH 8.0 (+1 m*M* EDTA) dissociate their clathrin coats into triskelions (arrows) upon adsorption to mica. × 102 000.

is eliminated in glycerol-sprayed samples (13, 24, 28, 29), presumably because triskelions are flattened by the air-drying involved in this technique.

When clathrin is presented to mica in buffers containing ≥25 m*M* of cations other than Tris, most trimers adsorb in much flatter, more extended, and more asymmetric forms (Fig. 4), and their arms, when bent at all, curve gently in the opposite, counterclockwise direction. Moreover, their vertices fail to display any pucker, even after freeze drying. Indeed, these forms are so flat that they are inadequately contrasted by replication at 24° (Fig. 5). Contrast is improved by replication at 6° (Fig. 6), and is optimized when both unidirectional and rotary shadowing are combined (as was done in Fig. 4). [It is important to note that although the majority of trimers in non-Tris solution adsorb to mica in disoriented or counterclockwise configurations, a minority persist in forming clockwise triskelions like those found in Tris (Fig. 4, arrowheads).]

We have performed a number of experiments to analyze the factor(s) that determine whether clathrin trimers adsorb "feet-first" (clockwise) or "vertex-first" (counterclockwise) (see the cover of this issue). The primary factor turns out to be their relative affinity for the mica surface. When their affinity is low, as in Tris, only those that contact the mica feet-first (clockwise) are able to adsorb. When their affinity is high, as in most non-Tris buffers, they can adhere in any orientation but display a predilection for vertex-first (counterclockwise) adsorption. Two observations lead to this conclusion. (1) Pretreatment of mica with polylysine, which greatly increases its affinity for

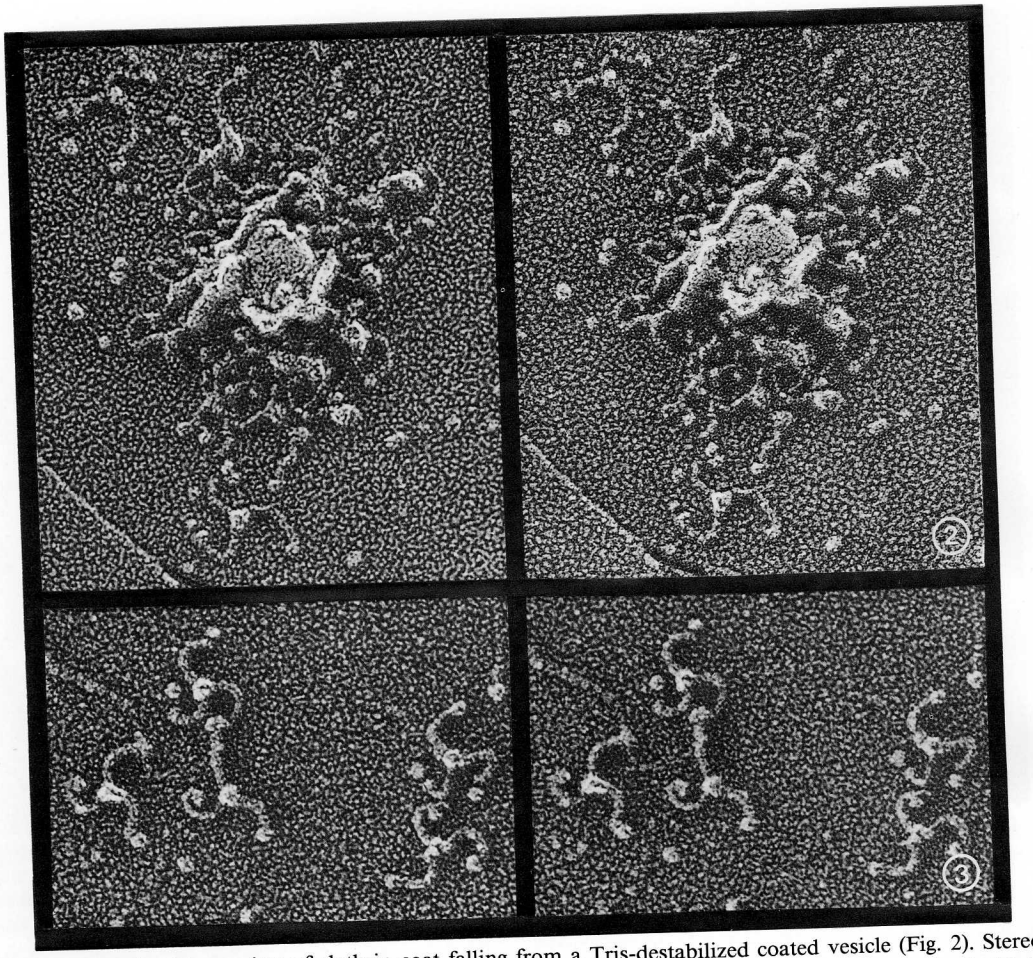

FIGS. 2 AND 3. Stereo view of clathrin coat falling from a Tris-destabilized coated vesicle (Fig. 2). Stereo view of clathrin trimers released from brain coated vesicles with 10 m*M* Tris, illustrating the clockwise "triskelion" orientation (with raised vertices) characteristic of low-affinity absorption to mica (Fig. 3). [These and all subsequent stereo figures should be viewed by the ocular divergence technique explained in Refs. (6) and (8), or by using a pocket stereo viewer.] Both fields × 250 000.

all proteins, invariably yields distorted images of clathrin trimers with most of their arms counterclockwise, even when they are presented in Tris buffer. (2) Lowering the ionic strength of any suspending medium to ≤25 m*M* strongly reduces mica's affinity for all proteins, and yields nothing but symmetrical "clockwise" images of clathrin trimers, even when the diluted buffer is *not* Tris.

2. *Molecular Dimensions of Triskelions*

Previous studies of clathrin trimers in the clockwise "triskelial" configuration recorded a total arm length of 44–50 nm (1, 14, 24, 26, 29). The terminus of each arm was described as a 5- to 7-nm knob (14) or a hairpin loop (26), and was found to disappear when triskelions were subjected to proteolysis, thus releasing 5- to 7-nm particles into the supernatant (14).

The present images of clathrin trimers freeze dried on mica add the following new information. Those that adsorb in the clockwise configuration (Figs. 1–3) are consistent with previous reports: their crooked arms measure ~47 nm *in toto* and display distinct 7 nm terminal "knobs." Trimers that

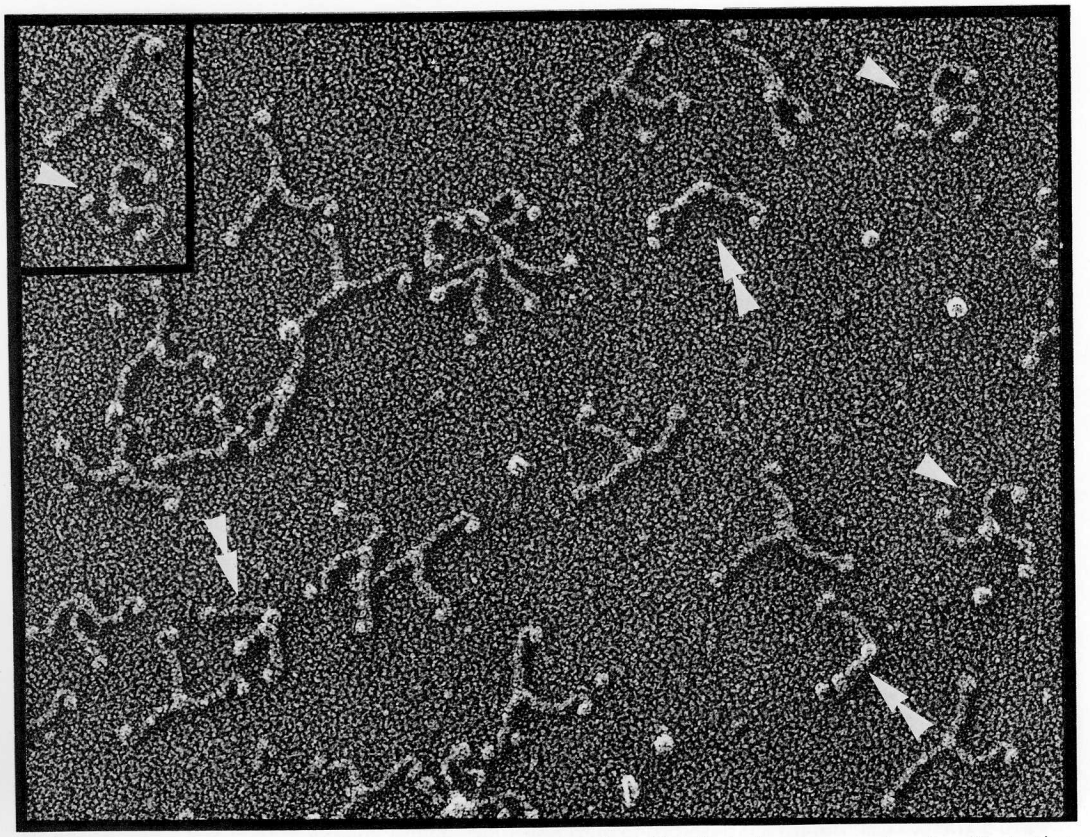

FIG. 4. Clathrin trimers maintained in 100 m*M* TEA buffer, pH 8.0, during exposure to mica, illustrating the predominantly counterclockwise orientation characteristic of adsorption under such high-affinity conditions. Some molecules still land in the clockwise "triskelial" orientation (arrowheads); a few even land on edge to give a side view of what may have been their original "pucker" (double arrowheads). × 230 000.

adsorb in the counterclockwise orientation, on the other hand, look significantly different (Figs. 4–6). Their arms look more extended and typically display distinct scroll-like "hooks" that twist in a clockwise direction before ending in 7-nm knobs. Proteolytic digestion releases the knobs into the supernatant (Fig. 7), and prolonged storage of triskelions at 4° sometimes results in the release of both the knob and the hook (Fig. 8, arrows).

Tracings of different "hooks" in our extended trimers (Fig. 9) offer a simple explanation for the relatively large differences in total arm length reported in the past literature (44–50 nm). When the hook is closed and the terminal domain lies against the side of the arm, one tends to measure out to the distal-most tangent of the hook, thus obtaining a relatively low value; but when the hook is unfurled, one tends to measure all the way around the curve and obtain a relatively high value. Figure 9 illustrates that 52 nm is the more accurate measure of total (extended) arm length.

3. Comparative Dimensions of Brain Coated Vesicles

Figures 10 and 11 show survey and stereo views of brain coated vesicles adsorbed to mica, then quick frozen and deep etched exactly as were the clathrin trimers described above. The size distribution of these vesicles is displayed at the top of Fig. 12. The histogram shows a peak (median) coat diameter of 60 nm; very few coats are small-

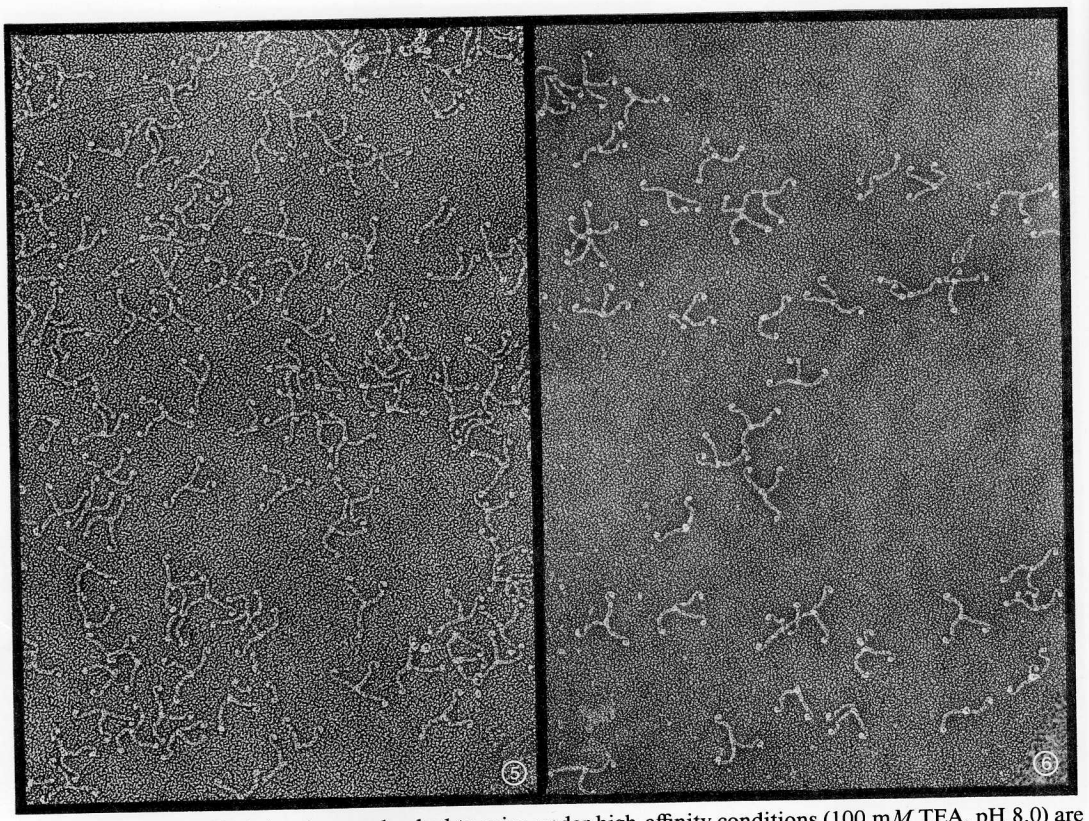

FIGS. 5 AND 6. Clathrin trimers adsorbed to mica under high-affinity conditions (100 m*M* TEA, pH 8.0) are so flat that 24° replicas (Fig. 5) yield relatively low-contrast images. Much improved contrast is obtained by replicating at 6° (Fig. 6). All other figures in this report represent a compromise at 12°, for technical reasons discussed in Ref. (8). Both fields × 105 000.

er than 50 nm; and a skewed tail extends to a maximum diameter of 92 nm. Since this is a surface-replica technique, we see only the upper halves of the baskets, so it is relatively easy to appreciate that the smallest ones (e.g., "S" in Fig. 10) are built like Form "B" of Ref. (2) (12 pentagons and 4 hexagons), whereas the predominant, medium-sized baskets ("M" in Fig. 10) are composed of 12 pentagons and 8 hexagons arranged in either of the Forms "A" or "C" observed in Ref. (2). Only a few of the largest ("L" in Fig. 10) appear to be built like Kanaseki and Kadota's predicted "vesicle in a basket" [a truncated icosahedron composed of 12 pentagons and 20 hexagons, like the standard soccerball; cf. Ref. 9]. The few that fall between the middle and large size-classes have more than 8 hexagons but often display 2 pentagons beside each other (cf. asterisk in Fig. 11), an arrangement never found in a full-sized soccerball. The implications of this size-distribution will be analyzed in Section 5, below.

4. *Molecular Dimensions of Reconstituted Cages*

Clathrin, obtained by dissolving brain coated vesicles in 2 *M* urea and purified by gel chromatography, will repolymerize into "empty baskets" upon dialysis against assembly buffer [low pH plus divalent cations; cf. Refs. (10, 11, 14, 17, 22, 30, 32)]. Previous thin-section and negative-stain studies of such reconstituted baskets have shown them to be variable in size, although sedimentation studies indicated two major classes at about 150 and 300 S (18, 30).

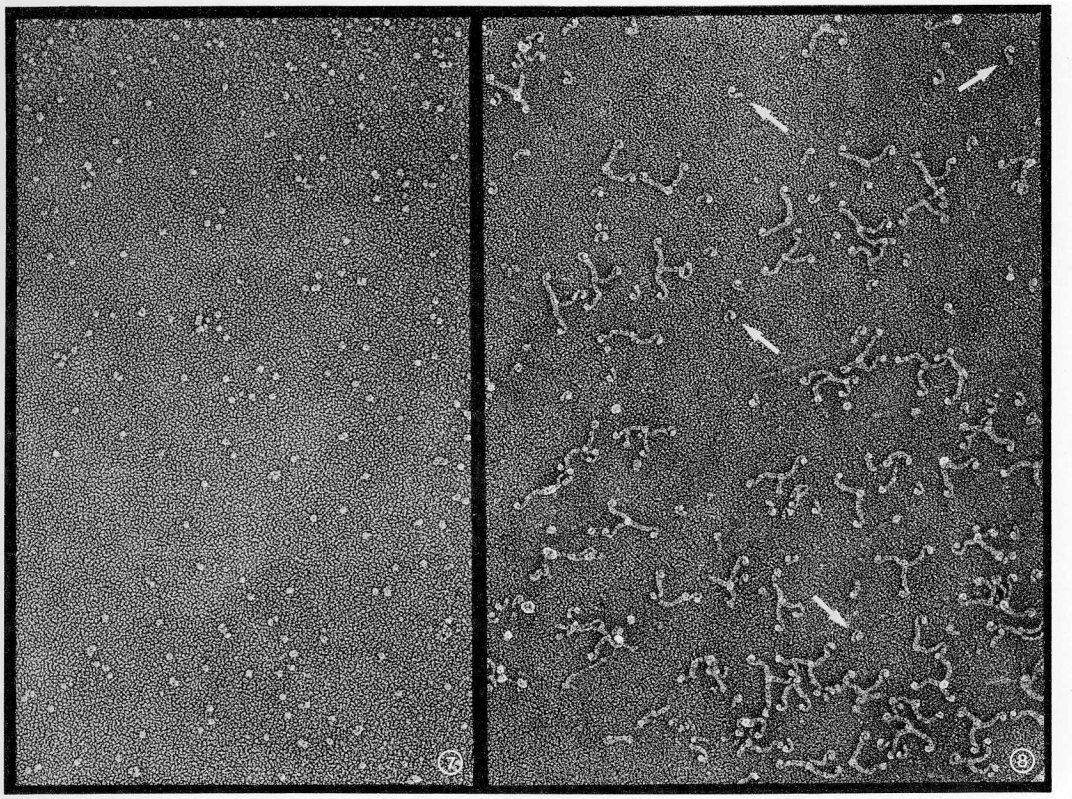

FIGS. 7 AND 8. Terminal domains of clathrin trimers released by brief proteolysis of reconstituted baskets [cf. Ref. (14)] form a uniform population of 5–7 nm granules (Fig. 7). Inadvertent proteolysis, due to prolonged 4°C storage of trimers, cleaved entire arms from many trimers and yielded scroll-shaped entities representing the distal portions of released arms (arrows) (Fig. 8). Both fields × 105 000.

These two classes are thought to correspond to the small "empty baskets" depicted in Ref. (2), on the one hand, and to the larger truncated icosahedra depicted in Ref. (9), on the other [cf. Refs. (3, 4, 10, 22, 25)].

In the present study, visualization of such reconstituted baskets has permitted a direct correlation of their polygonal composition with their respective sizes (Fig. 13). In fact, size histograms from fields such as Fig. 13 display *three* major classes, not two. As shown in Fig. 12 (third row), these center around 55, 80, and (more broadly) 110 nm. Negatively stained aliquots of the same preparations (Fig. 14) display the same small-medium-large differentiation (Fig. 12, fourth row), but with the added caveat that the baskets are flattened by the latter technique (compare Figs. 15 and 16). Closer inspection of the polygonal composition of freeze-etched baskets reveals that the smallest are rich in juxtaposed pentagons, again like Form "B" of Ref. (2), whereas the middle-size class (~80 nm) approximates a truncated icosahedron (the "soccerball"). As diagrammed in Fig. 17, the pentagons in a soccerball should always be separated from each other by the "seams" between hexagons. Actually, as seen also in the larger of our brain coated vesicles, our middle-sized empty baskets often display two pentagons next to each other (Fig. 16, arrow), so they must have somewhat fewer than the predicted 20 hexagons of the perfect soccerball.

The largest of our reconstituted baskets have no equivalent in the original coated vesicle preparations from brain, but approach the sizes of coated vesicles found,

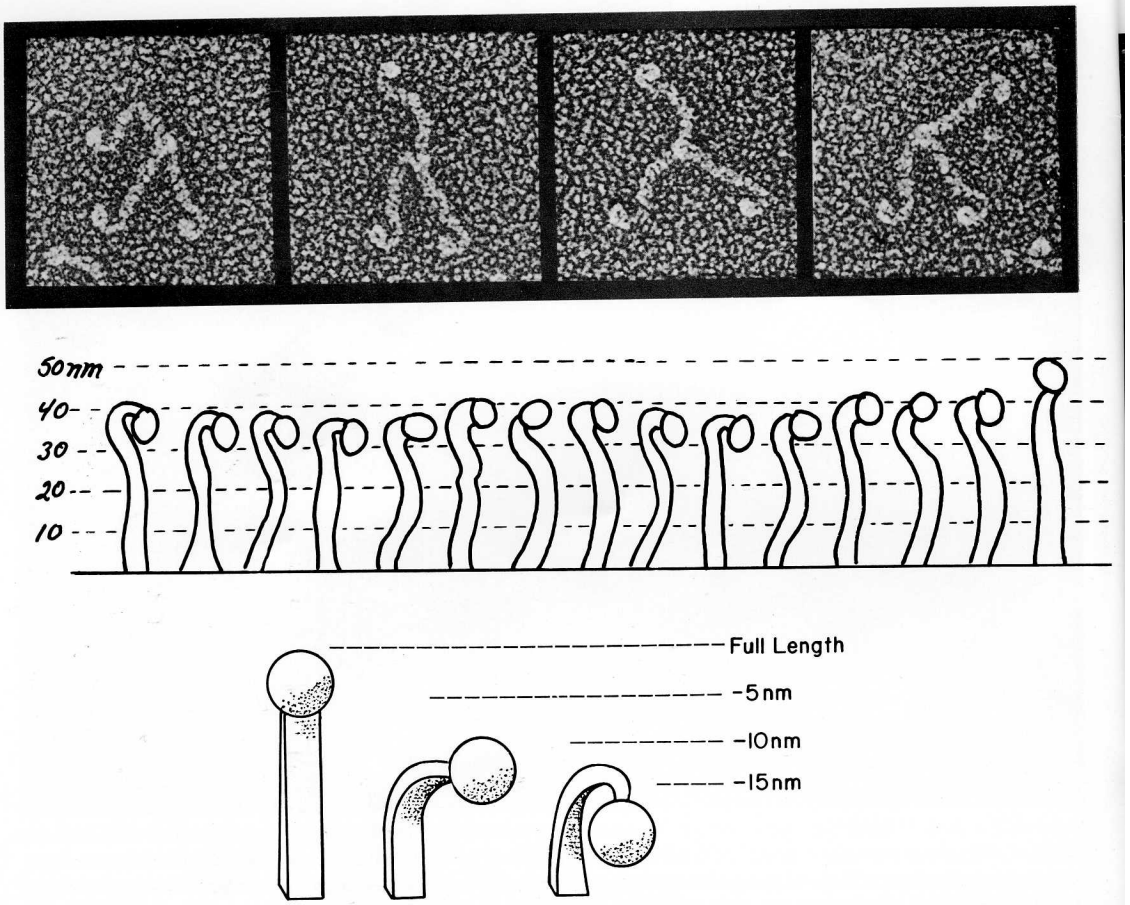

FIG. 9. Examples of trimers with distinctly scroll-shaped terminal domains (above, at × 420 000); camera lucida tracings of arms selected to illustrate their variable degree of curling (center, at 10^6 ×), and a schematic drawing of how arm-length measurements will be reduced by measuring only to the distal tangent of the hook (below).

for example, in hepatocytes, fibroblasts, and oocytes (6, 23). Figure 17 illustrates that if these conformed to the same architectural principles as smaller baskets, they would most likely be built exactly like papilloma–polyoma viruses [cf. Ref. (16)] which have perfect icosahedral symmetry with two hexagons separating each pentagon. Given the dimensions of the smaller baskets discussed above, such icosahedral forms should have an overall diameter of ~120 nm. Actually, reassembled baskets are rarely large enough adopt to this symmetry exactly, and the largest turn out to display a number of lattice dislocations. As seen at the arrowhead in Fig. 16, these often result in the formation of odd seven-sided facets like as those seen in flat clathrin lattices *in situ* (6). Such dislocations are usually associated with abrupt changes in coat curvature, suggesting that the largest baskets may form by coalescence of two (or more) fragments with

FIG. 10. Coated vesicles isolated from bovine brain and adsorbed to mica before freeze drying and rotary replication. Larger pale spheres are membranous contaminants. A few baskets are singled out as being among the smallest (S), the largest (L), and the median (M). × 150 000.

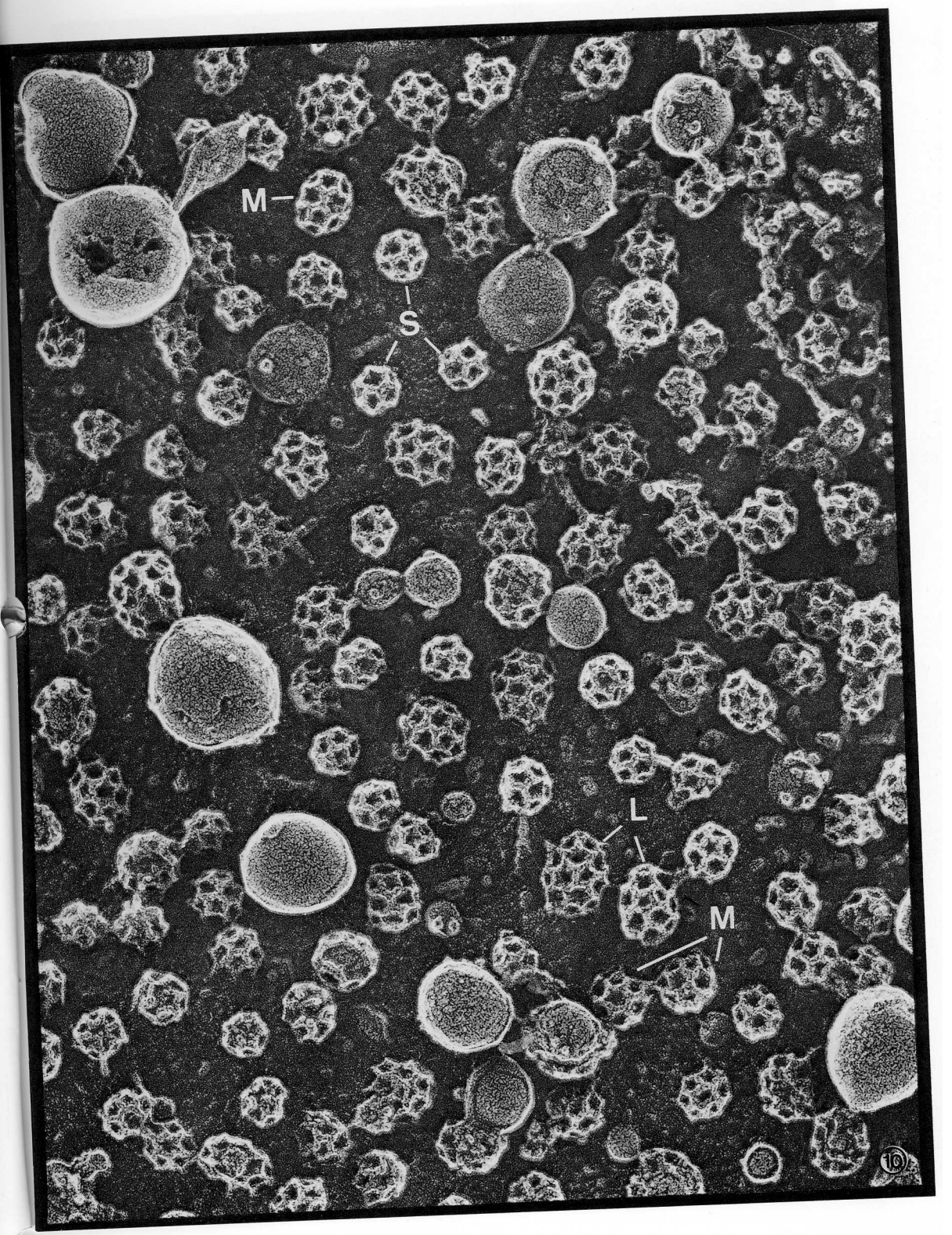
M
S
L
M

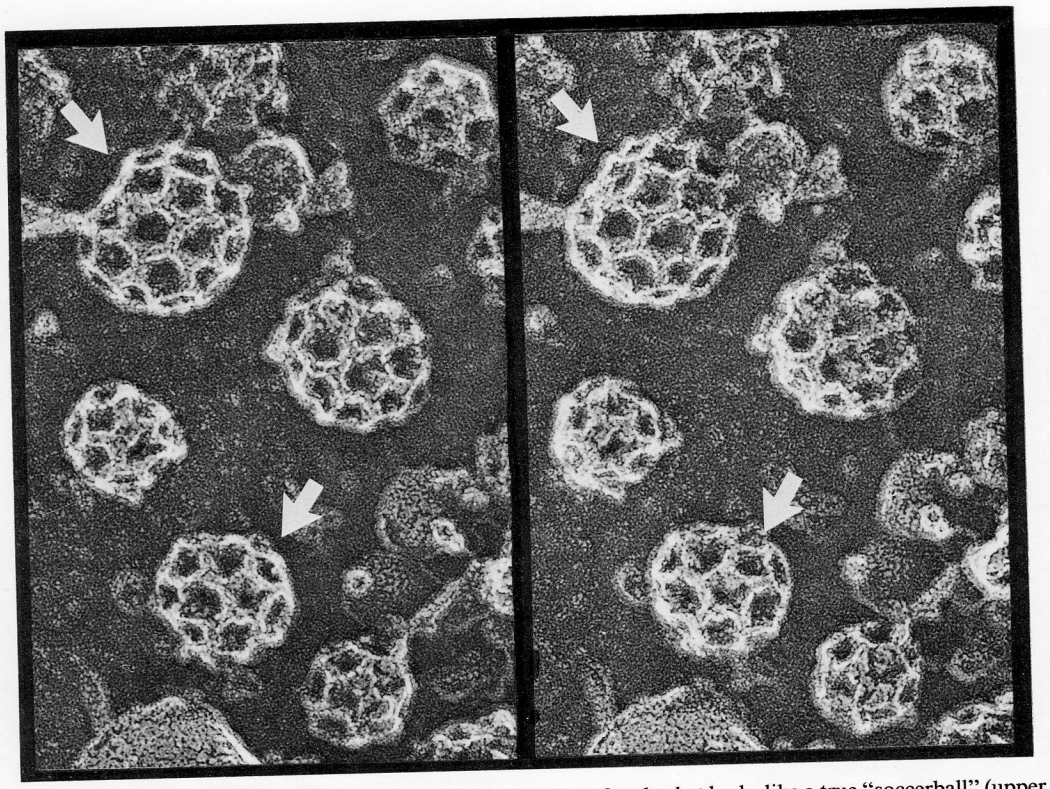

FIG. 11. Stereo view of the above coated vesicle preparation. One basket looks like a true "soccerball" (upper arrow); a slightly smaller basket of "intermediate" configuration (lower arrow) is discussed in the text. × 250 000.

differing radii. We have never seen such "siamese twins" in the original coated vesicle preparations from brain; hence we presume they represent "mistakes" generated during *in vitro* repolymerization.

5. *Determining Edge Length in Clathrin Polymers*

The dimensions offered for the various polyhedral forms in Fig. 17 are based on the supposition that the overall size of any polygonal basket will depend on (1) the dimensions of its component polygons and (2) its total number of polygons. With this in mind, the basket size-measurements presented above lead to a specific prediction for the dimension of the individual clathrin polygon. To generate either truncated icosahedra (12 pentagons and 20 hexagons) of ~76 nm, or smaller forms (12 pentagons and 8 hexagons) of ~60 nm, the edge (ℰ) of each polygon should ~ 15.5 nm. [This value was obtained by calculating the surface areas of spheres of different diameters and

FIG. 12. Histograms of clathrin-basket diameters illustrate that three size-classes are discernible in regrown baskets, but that brain preparations contain mostly the smallest class. Negative staining yields consistently larger diameters, due to flattening of the baskets (cf. Figs. 15, 16). A correlation of the freeze-etch numerology with predictions based on geometry is discussed in the text and summarized in Fig. 17.

FIGS. 13 AND 14. Empty baskets generated by slow dialysis of pure clathrin against a polymerizing buffer [cf. Ref. (14)], then either freeze-etched (Fig. 13) or negatively stained (Fig. 14). Both fields printed at the same magnification to illustrate that the baskets look larger after negative staining. × 110 000.

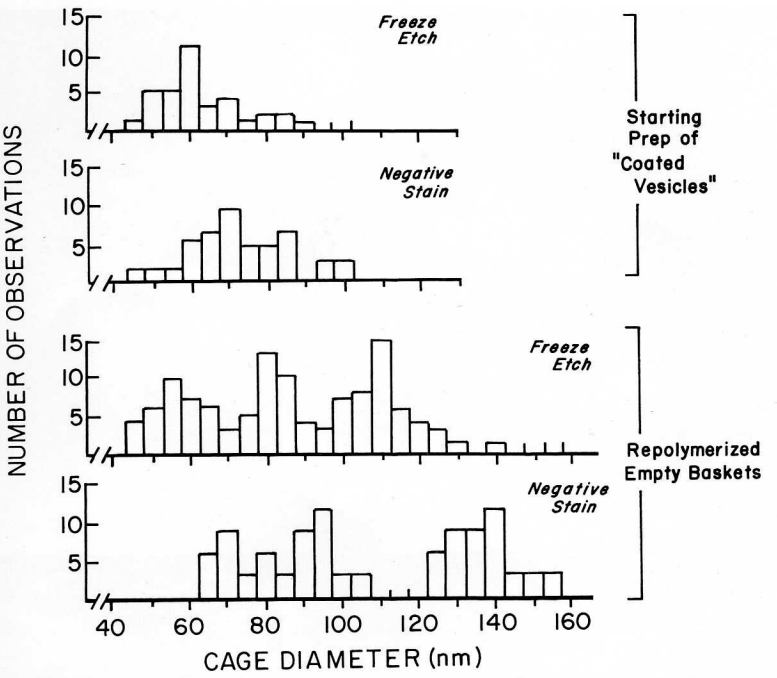
NUMBER OF OBSERVATIONS
15
10
5
Freeze Etch
Negative Stain
Starting Prep of "Coated Vesicles"
Freeze Etch
Negative Stain
Repolymerized Empty Baskets
40
60
80
100
120
140
160
CAGE DIAMETER (nm)

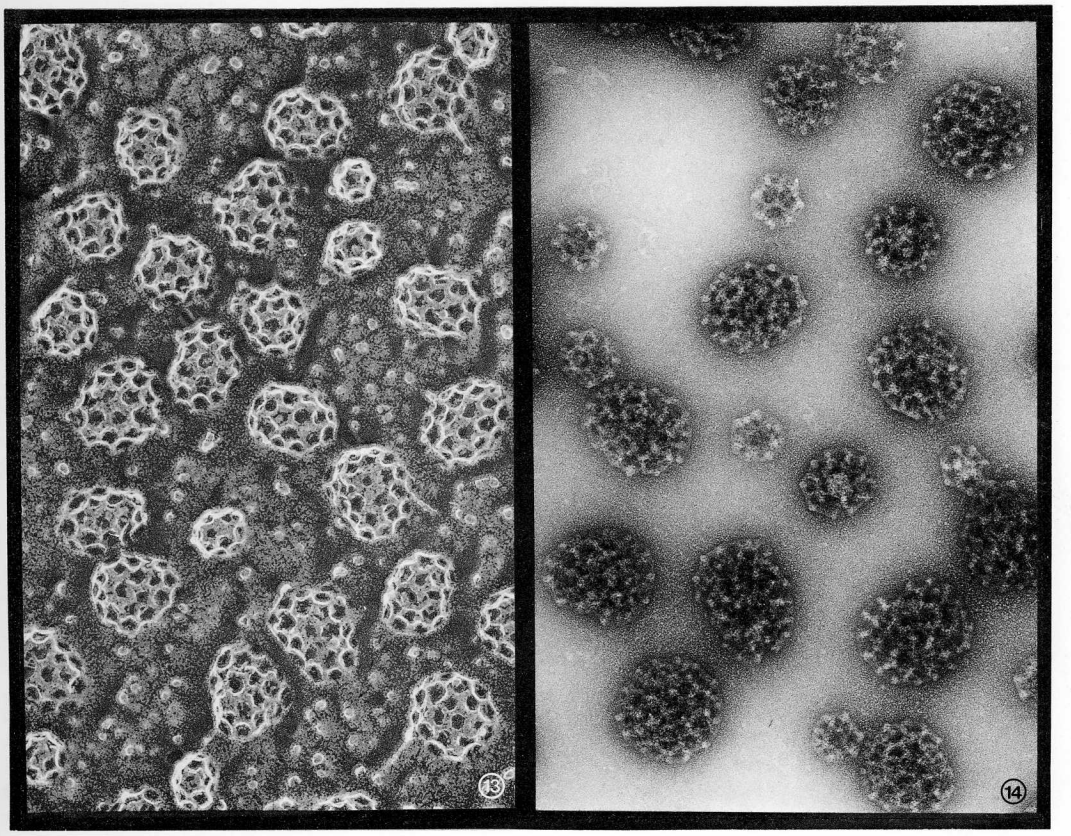
13
14

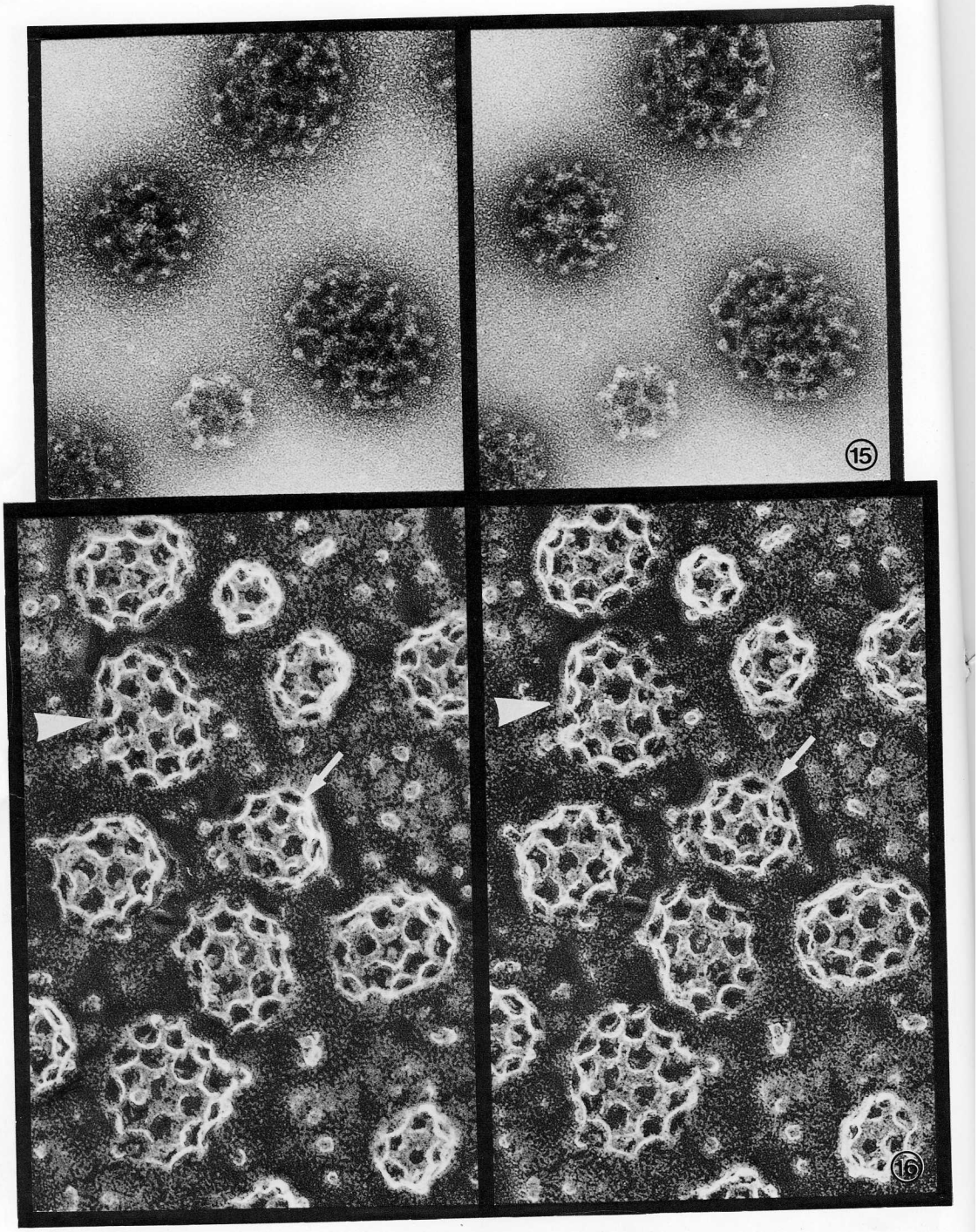

FIGS. 15 AND 16. Stereo views of repolymerized baskets after deep-etching (Fig. 15) versus negative staining (Fig. 16), again printed at the same magnification to permit direct comparison. Stereo viewing illustrates that the negatively stained baskets are extremely flattened compared to the deep-etched ones. (Simple geometrical calculations dictate that complete flattening would yield a disk 40% larger in projected diameter than the original basket, assuming its surface area remains constant.) The arrowhead in Fig. 16 denotes a lopsided basket with a

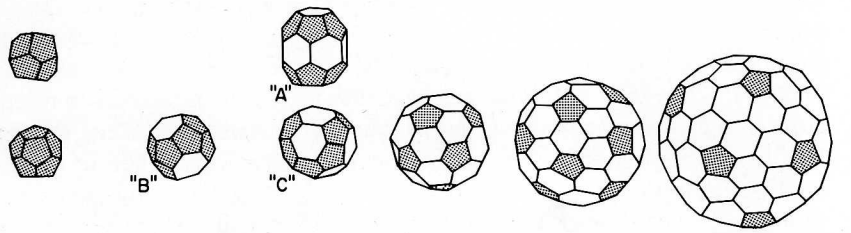

	Dodecahedron	Type "B"	Types "A" and "C"	Truncated icosahedron (brain)	(Liver)	Full icosahedron (fibroblasts)
No. of hexagons	0	4	8	20	30	60
No. of vertices	20	28	36	60	82	140
Predicted diameter (nm)	40	50	60	76	90	120
Predicted weight (MD)	13	18	23	38	53	77
No. of "facets" in deep etch	3–4	4–5	7–8	10	14	24
No. of "spikes" in neg. stain	4–5	5–6	6–8	8	12	16–17

FIG. 17. Schematic drawings of several symmetrical basket designs of progressively larger sizes. The table below catalogs their expected complement of polygons, expressed as a number of hexagons in addition to the 12 pentagons always needed to form a closed polygonal shell. (Pentagons are shaded in the drawings.) Also recorded are their number of vertices, which would be equivalent to their total complement of clathrin trimers if current packing models [Refs. (1, 12)] are correct. Assuming further that a trimer weighs 640 kDa [Refs. (12, 26)], these numbers lead directly to predictions of total molecular weight for each sized basket (expressed in megadaltons). Predicted diameters are obtained by assuming that the length of each edge in a polygon ($\mathcal{S}$) is 15.5 nm (see text for details). This value was first chosen to yield diameters that would fit the data in Fig. 12, then later confirmed by direct measurement. Also listed, to assist correlating these predictions with past observations in the literature, are the number of polygonal facets that would be easy to see in surface replicas like those produced in freeze etching (i.e., one-sided views), and the number of peripheral "spikes" or "knobs" that would be seen in negatively-stained or thin-sectioned coats (i.e., translucent projection views).

comparing these values with geometrical determinations of the surface area of individual pentagons ($\sim 1.7\ \mathcal{S}^2$) and hexagons ($\sim 2.6\ \mathcal{S}^2$); a more specific mathematical formulation reaching the same conclusion is found in Ref. (25), page 1720.]

Matching this prediction, our actual measurements of vertex-to-vertex distances in baskets such as those in Figs. 11 and 14 yield a mean +SE for $\mathcal{S}$ of 15.5 ± 0.6 nm (n = 87). As noted under Materials and Methods, we made these measurements while viewing the cages stereoscopically, to be sure that we did not consider inclined polygons whose edges would appear foreshortened. Furthermore, we obtained an identical value of 15.5 ± 0.7 nm by measuring $\mathcal{S}$ in the broad, flat, purely hexagonal patches of clathrin that we find in fibroblasts [Ref. (6)]. (Of course, $\mathcal{S}$ would be the same regardless of whether the edge is part of a pentagon or hexagon, or part of a small, large, or infinite-diameter basket.) This value is substantially less than the currently accepted value of 18.5 nm (3, 10, 21, 25), which was derived from negatively stained preparations (1, 21). How-

lattice discontinuity that contains a 7-sided polygon like those seen *in vivo* [cf. Ref. (6)]. The arrow in Fig. 16 denotes a basket with two adjacent pentagonal facets, discussed in text. × 185 000.

ever, measuring the micrographs in Ref. (1) ourselves, we find a range of values of $\mathcal{S}$ from 18.0 to 15.4 nm with a mean +SE of 16.7 ± 0.8 nm (n = 78). Furthermore, measuring our own negative stains of basket fragments photographed in the same microscope as our replicas gave a range of 14.5–16.0 nm (n = 18), and our previously published negative stains of clipped baskets [Ref. (14)] gave a range of 13.6–15.6 nm with a mean of 14.3 ± 0.7 nm (n = 60). Thus we conclude that the value of 15.5 nm is a more accurate estimate of $\mathcal{S}$. This will affect our predictions about clathrin assembly, to be presented in the Discussion.

6. *Analysis of Cage Construction*

In experiments designed to understand how triskelial "pinwheels" might assemble into polygonal basketworks, Crowther and Pearse attempted to trap assembly intermediates on electron microscopic grids and visualize them by negative staining (1). They obtained images of hexagons and pentagons, surrounded by incomplete polygons, that occasionally appeared to consist of individual triskelion arms. This led them to a specific model for basket assembly (1). However, due to contrast limitations in negative staining, these authors did not succeed in showing exactly how many clathrin arms go into a completed strut in the basketwork, nor exactly how the arms overlap and course through the basketwork.

We have attempted similar assembly experiments, visualizing the products by deep etching. However, as Figs. 18–20 illustrate, our results were also ambiguous. Two problems arose. First, when we attempted to capture intermediates at early times, the mica invariably became saturated with an obscuring layer of unreacted trimers. Second, when we let the reaction proceed long enough to reduce the relative concentration of unreacted trimers, we obtained almost nothing but completed baskets. Furthermore, the few species that looked to be assembly intermediates displayed a marked tendency to depolymerize upon adsorption to mica (Figs. 18–20). To demonstrate this point, Figs. 21–23 illustrate intentional *disassembly,* generated by adsorbing complete clathrin baskets to mica under destabilizing conditions. Here, the frayed edges look subjectively different than during assembly, in that they show many radiating arms; nevertheless, their original pattern of organization cannot be discerned. The images provide nothing more than a sense of the relative calibre of intact cage struts (7 nm) versus individual trimer arms (~3.5 nm).

A curious result was obtained in a few reassembly experiments that were designed to go to completion (Fig. 24). Such preparations of course display a great abundance of finished baskets, but some also contain many small basket fragments (Fig. 24, arrowheads) composed of no more than one or two polygons. When present, these fragments do *not* display the halo of uncommitted trimer arms expected from the model of clathrin assembly proposed in Ref. (1). Instead, the struts extending out from them appear too stout and end too abruptly to fit the model. However, attention to the remaining uncommitted trimers in these unusual preparations suggests an explanation for this bluntness. The arrows in Fig. 24 point to several molecules that have been clipped into two- or one-legged entities. We thus suspect that in these experiments, certain growing networks incorporated such proteolyzed species, the result being an arrest of assembly and an accumulation of truncated "dead-end" basket fragments.

7. *Determining the Contents of Brain "Coated Vesicles"*

When brain coated vesicles are compared with reconstituted "empty baskets" after negative staining (Figs. 25 vs 26), the former are invariably found to contain some sort of stain-excluding core, even though the cores in the smallest ones are too small to represent any known type of membrane vesicle (5). Indeed, only the largest baskets contain clear-cut bilayer vesicles. Freeze fracture confirms this impression. Thus when

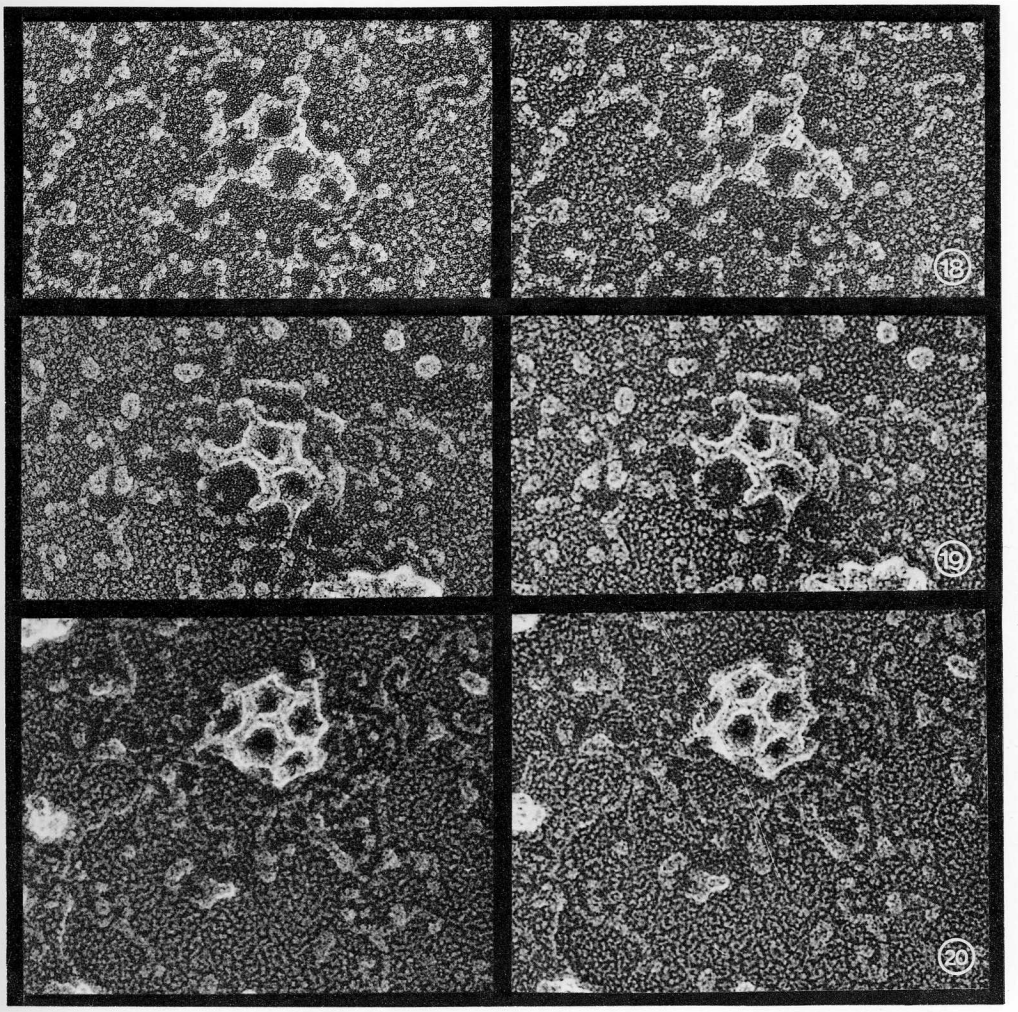

FIGS. 18–20. Incomplete polygonal networks captured during clathrin polymerization (by acidifying a solution of pure clathrin and immediately applying it to mica). As discussed in the text, these intermediates lack the expected complement of uncommitted triskelion arms. × 250 000.

small vesicle-containing particles such as Semliki Forest viruses are adsorbed to mica and freeze fractured, their internal membranes are uniformly exposed (Fig. 27). By contrast, when brain coated vesicles are so fractured, only the largest reveal an enclosed bilayer vesicle (Fig. 28, arrow). The rest fracture straight through, often accompanied by some plastic deformation typical of pure protein assemblies, yielding images of granular, nonmembranous cores (Figs. 28, 29).

The contents of brain coated vesicles have been visualized in two additional ways. One involves placing them on polylysine-coated mica, which we find induces their baskets to fall off during adsorption (Fig. 30). When bilayer vesicles are harbored within the baskets, they are thereafter readily discerned, either as hollow "craters" if they rupture (Fig. 30, arrows) or else as relatively smooth spheres (Figs. 31 and 32, arrows). Such images, however, are quite rare; most baskets simply fall apart into "heaps" of triskelions with no membranous components inside.

The other way to visualize the contents

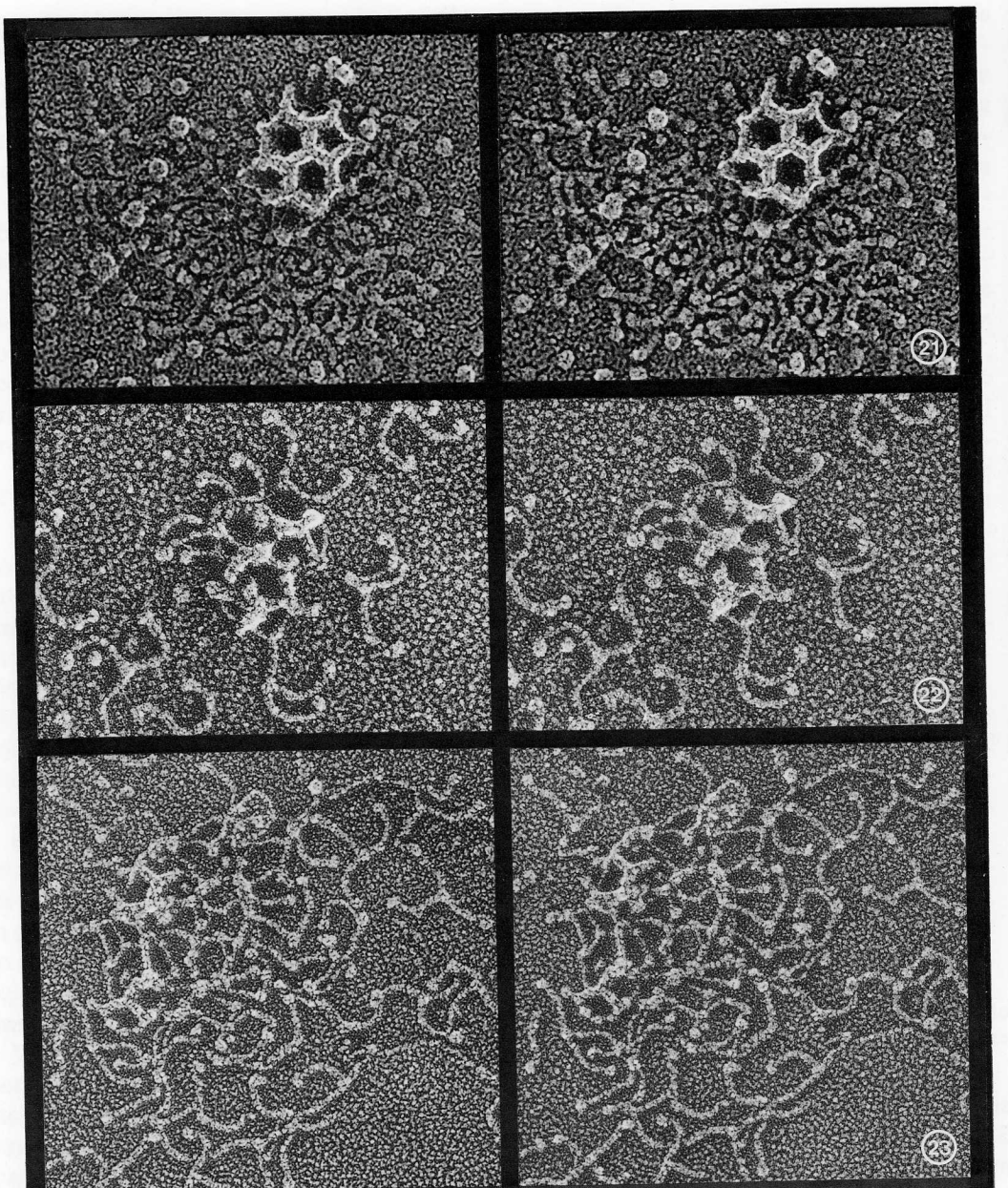

FIGS. 21–23. Polygonal networks of clathrin trapped during depolymerization, either by absorption to polylysine-treated mica (Figs. 21 and 22) or by raising the pH after adsorption to mica (Fig. 23). In contrast to Figs. 18–20, intermediates in depolymerization do appear to be surrounded by overlapping trimer arms. × 250 000.

of brain coated vesicles is to expose them to Tris (10–100 m*M*, pH 8) immediately before adsorbing them to untreated mica. As was shown in Figs. 1–3 above, this treatment not only causes their coats to dissociate but also reveals an internal vesicle when one is present. Again, the majority of the baskets in our preparations lack such internal vesicles, as would be expected from the predominance of smaller sizes (cf. Fig. 12).

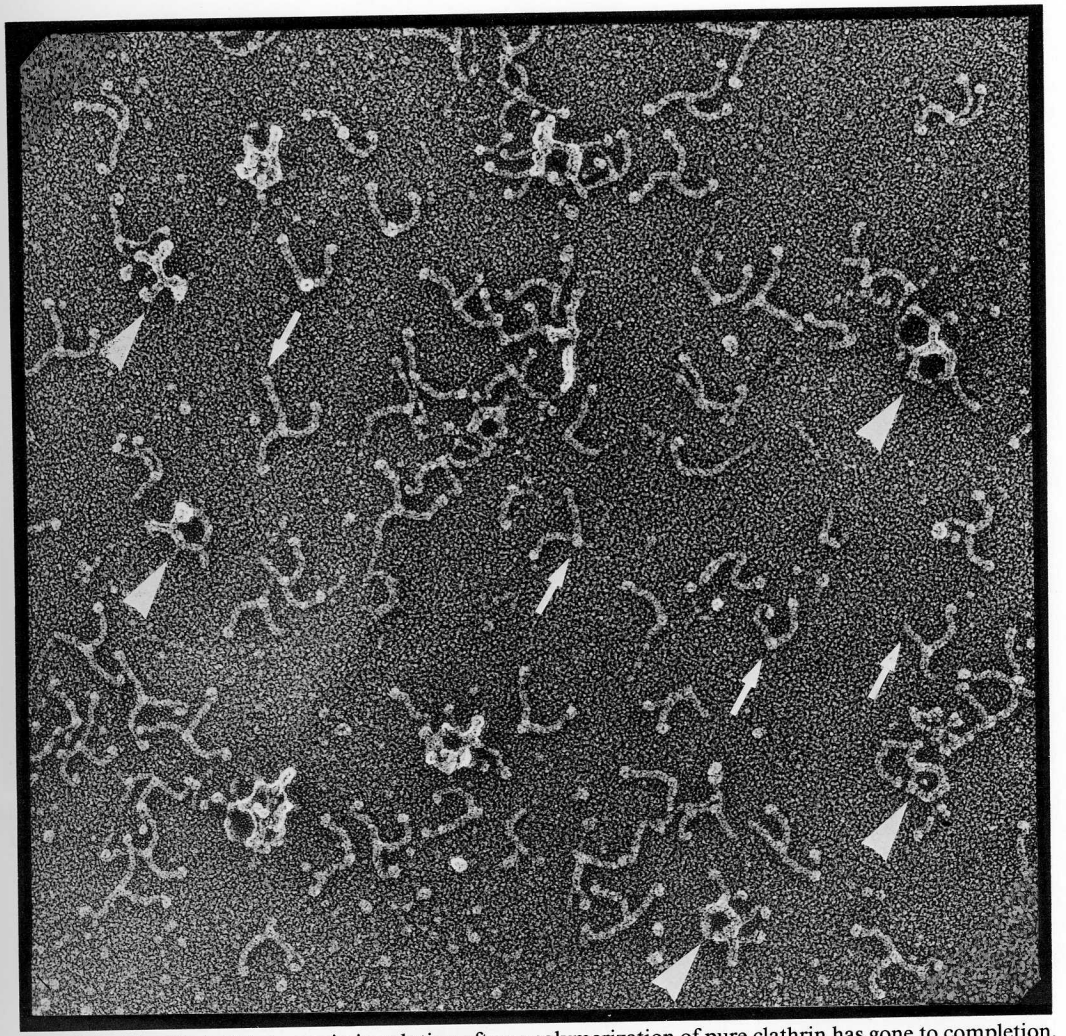

FIG. 24. The "dregs" that remain in solution after repolymerization of pure clathrin has gone to completion. The remaining polygonal fragments (arrowheads) are not surrounded by the expected number of free clathrin arms. Moreover, many of the unreacted trimers (arrows) display one or more clipped arms, suggesting that proteolysis has occurred.

Biochemical analysis of the proteins that purify with clathrin in such brain "coated vesicle" preparations suggests that the internal masses in the smaller baskets may include substantial amounts of the so-called "assembly polypeptides" (10, 33), which might have artificially nucleated basket formation from clathrin solubilized during the initial brain homogenization or during sucrose centrifugation. Indeed, we invariably observe internal masses in baskets reassembled in the presence of assembly polypeptides after either by negative staining or freeze fracturing (work in progress with Dr. James Keene, Temple Univ.). On the other hand, we also suspect that at least some of the internal mass is contributed by the distal portions of the triskelion arms themselves, a possibility evaluated in the next section.

8. Evidence that Triskelion Arms Point into the Basket

The current model of clathrin assembly holds that each triskelion arm participates

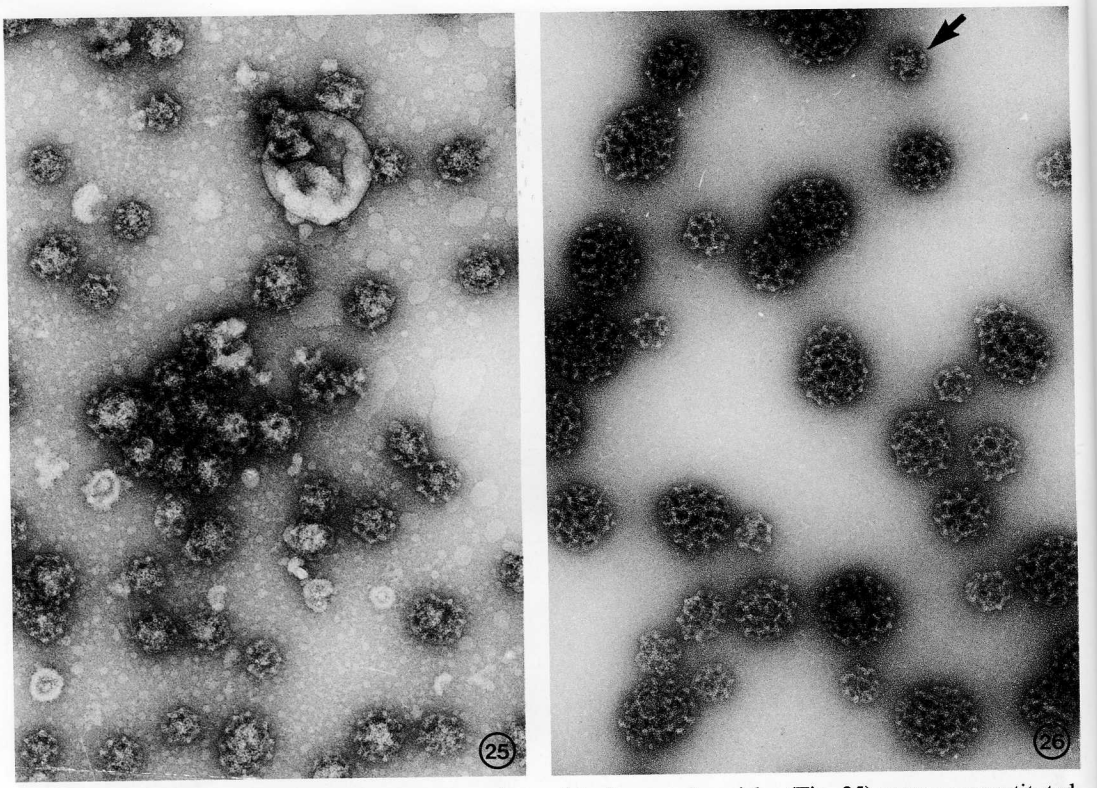

FIGS. 25 AND 26. Negatively stained preparations of brain-coated vesicles (Fig. 25) versus reconstituted baskets (Fig. 26), illustrating that stain-excluding "nuggets" occur in even the smallest of the baskets in brain preparations but are rarely found in reconstituted baskets (one only at the arrow in Fig. 26). Both figures × 73 000.

in forming two struts [so that each strut is composed of four overlapping arms (1, 4, 27)]. Since we now find that each strut in a polygon measures 15.5 nm while each arm measures 52 nm, this model would predict that after traveling around two sides of the polygon, some 20 nm of each arm would be "left over." An obvious possibility is that this extra length might extend inward, in which case we have begun to realize that it should almost fill the interior of the smaller baskets (Fig. 33).

In theory, the most straightforward test of this possibility should come from freeze-fracture images of reconstituted baskets; these have no associated assembly polypeptides or lipids, so their centers should reveal inward-directed triskelion arms if they indeed exist. Figure 34 illustrates that upon freeze fracture, such reconstituted baskets actually appear to be relatively empty. However, upon comparison with freeze-fracture images of clipped baskets (Fig. 35)—baskets whose terminal domains have been

FIGS. 27–29. Semliki Forest viruses (Fig. 27, kindly provided by Dr. Ari Helenius, Yale Univ.), adsorbed to mica and then freeze-fractured to expose their internal membranes, either in convex (P face) or concave (E face) views. Icosahedral symmetry of the capsids on unfractured viruses is visible in the upper left-hand corner. Two stereo views of freeze-fractured brain "coated vesicles" (Figs. 28 and 29, in this case, from a preparation kindly provided by Dr. Daniel Branton, Harvard Univ.). Here, fracturing exposes dense granular cores inside almost all the baskets, even the smallest. Only a very few baskets (and only the largest, cf. arrow in Fig. 28) contain a bilayer vesicle that fractures smoothly like the membranous viruses in Fig. 27. All fields × 120 000.

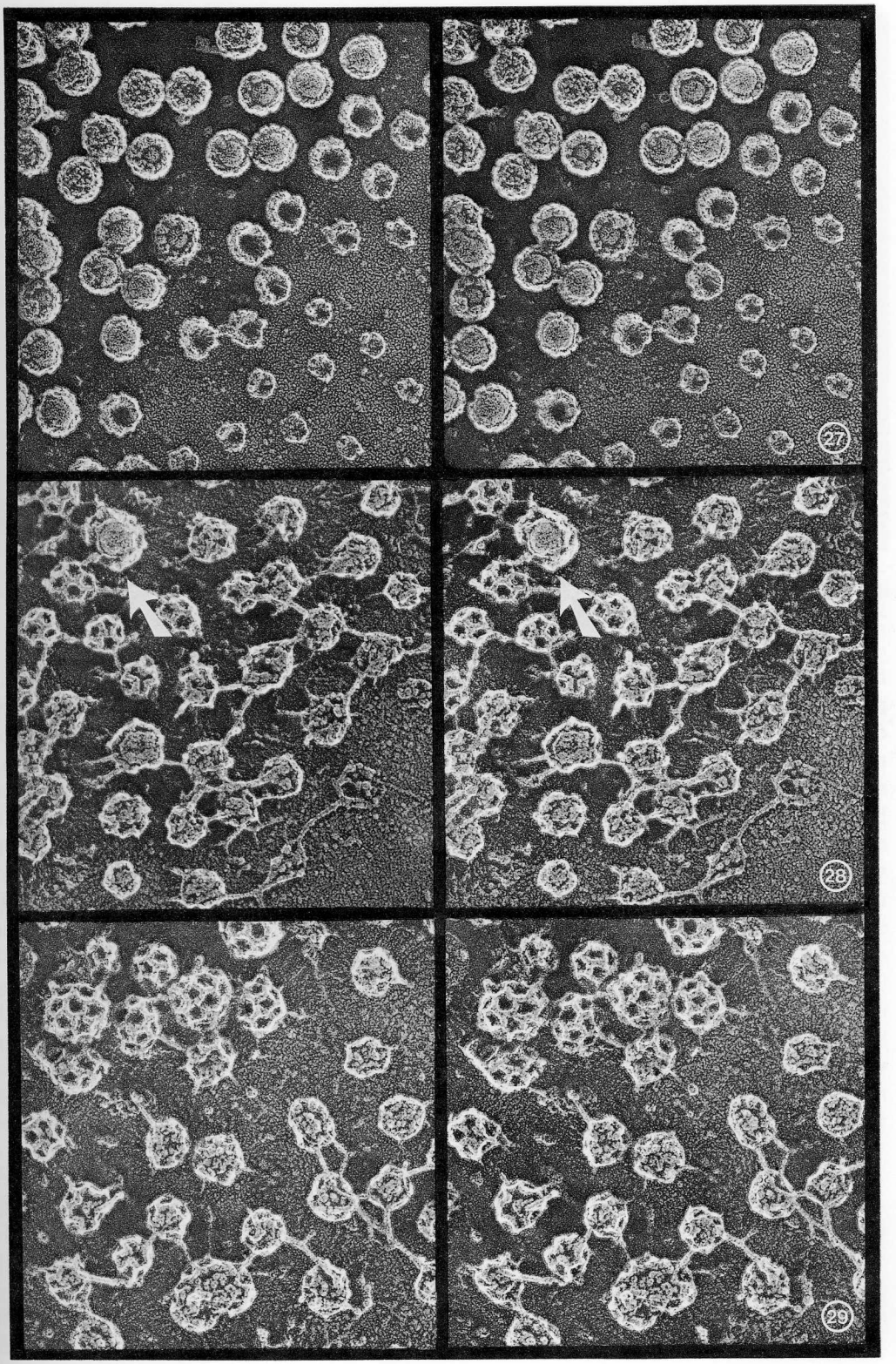
27
28
29

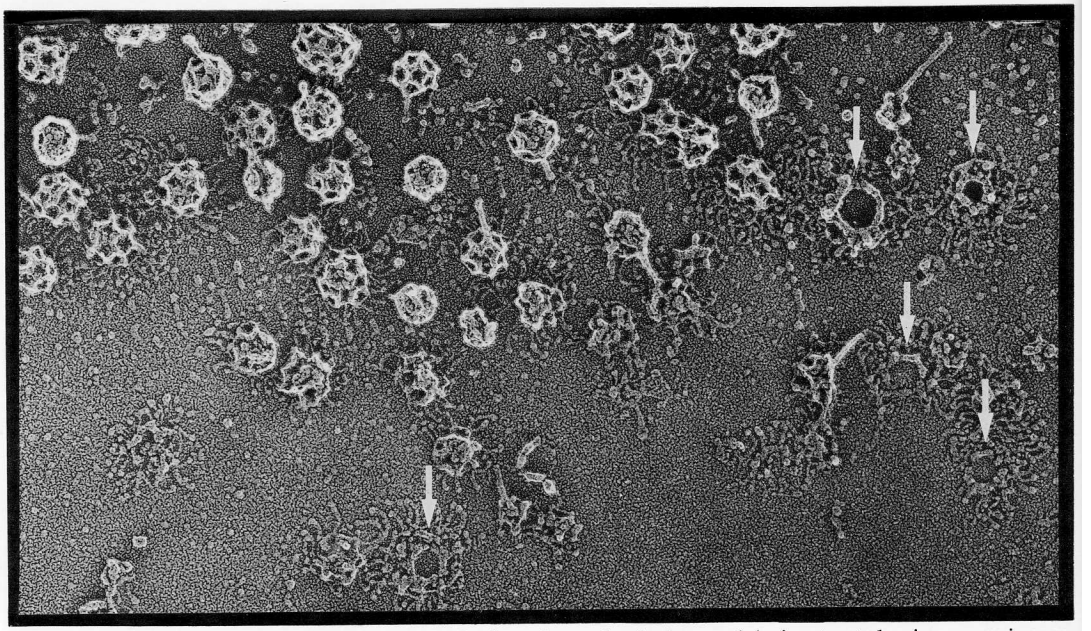

FIG. 30. Coated vesicle preparation from brain, when adsorbed to polylysine-treated mica, experiences dissociation of the clathrin baskets and rupture of the internal vesicles (to form the craters seen at the arrows). × 105 000.

released by proteolysis (14)—it becomes apparent that the walls of intact baskets are demonstrably thicker than clipped baskets, measuring some 15 nm versus only 8–10 nm after clipping. [It is worth remembering here that the apparent "gap" between basket and internal membrane in *bona fide* coated vesicles measures 10–20 nm, depending upon how the sample is prepared for microscopy (3, 6, 9, 23).] This can best be discerned and quantitated by viewing such walls in 3-D, as in Figs. 36 and 37. This "thinning," which may explain why clipped baskets collapse so readily during negative staining (14), provides direct evidence that the distal parts of clathrin arms extend inward.

DISCUSSION

Understanding the mechanism of coated vesicle formation, or more restrictedly, the mechanism of clathrin basket formation, awaits more definitive determination of the configuration of clathrin trimers in solution and their final packing geometry in completed baskets. While bearing analogies with virus capsid assembly, this self-assembly process will probably turn out to be more like the formation of the extracellular matrix in eukaryotes, where extended fibrous molecules are the starting materials and the final products display considerable variability in size, polygonal composition, and curvature. The marked regional differentiations shown by extracellular coats are also analogous to the strict segregation of clathrin coats to certain receptor-rich, "budding" regions of membrane; in both situations, the controlling role of membrane linkages must be paramount.

Deep etching provides a vital visual link between protomer and product in both these situations. It permits direct comparison of their relative geometries, since it subjects both to the same rigors of specimen preparation for electron miscroscopy. Moreover, since it is conjoined with metal replication, it provides the requisite high contrast *en face* surface views of what are essentially extended, planar assemblies.

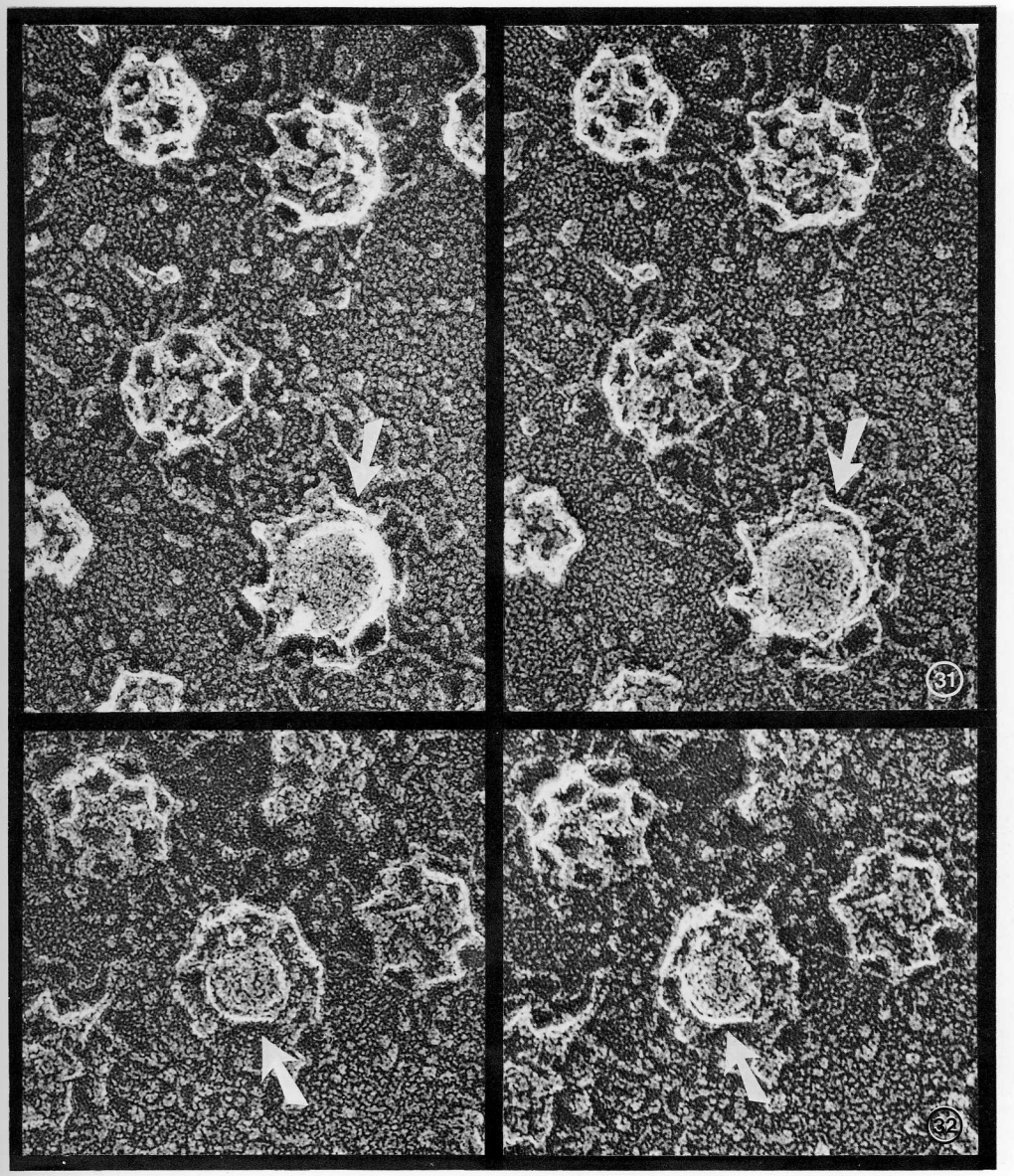

FIGS. 31 AND 32. Stereo views of brain coated vesicles dissolved by contact with polylysine-treated mica, showing two examples of the internal vesicles revealed thereby (arrows). Such membranous cores are seen in only a few percent of all baskets (and only the largest ones). Both fields × 250 000.

Current shortcomings of the technique, highlighted in the present study, include the need to display the protomers on an adsorptive surface (which can alter their *in vitro* geometry), and the intrinsically low resolution of the metal replicas (which obscures the details of packing in the final polymer). Thus clathrin trimers are shown to assume two very different configurations when adsorbed to mica, depending on the ionic composition of the medium in which they are suspended and the resultant surface charge of the mica, warning us that any image of an adsorbed protein, by whatever

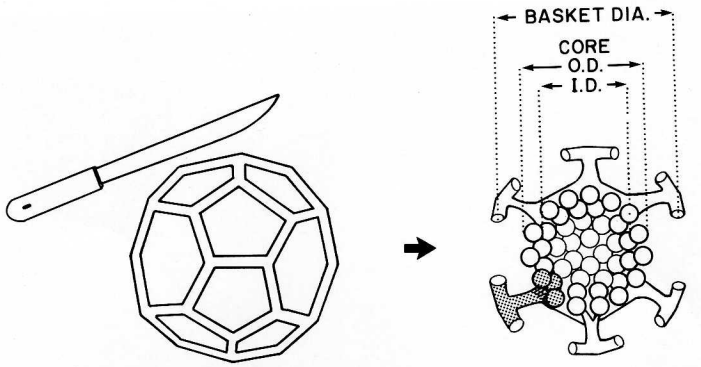

	Smallest (dodecahedron)	Type "B"	Types "A" and "C"	Truncated icosahedra
Number of terminal domains	60	84	108	180
Basket diameter (nm)	40	50	60	76
"Shell-like" core				
Outer dia. (nm)	26	36	46	62
Inner dia. (nm)	14	24	34	50
(% Occupancy)	(>100%)	(90%)	(60%)	(54%)
"Solid" core dia. (nm)	24	26	29	34

FIG. 33. Diagram of the "core" of protein that should be found in freeze-fractured baskets [specifically, the small 50 nm "B" type of Ref. (2) is shown here], if the terminal 15–20 nm of the trimer arm extends *inward* from the polygonal shell. The stippled portion is intended to illustrate that 3 trimer arms should extend in from each vertex, thus contributing three ~6 nm "terminal knobs" to a protein-rich "core." The table below presents the expected dimensions of this core of clathrin-termini for the four smaller baskets shown on the left of Fig. 17, assuming that each terminal domain is a 6-nm sphere. Core-size is expressed first as the i.d. and o.d. of a spherical "shell" (in case it were arranged internally as shown in the diagram above). *Note that the inner diameter of this shell would dictate the size of the membrane vesicle that could be enclosed,* and is smaller than brain synaptic vesicles for all forms except the truncated icosahedra, which were recognized early-on to be the basic design of brain coated vesicles [Ref. (9).]. [Percentage occupancy simply indicates how "complete" the wall of the hollow core would be, vis-à-vis the packing of knobs (terminal domains) in the above diagram. Note that the smallest possible baskets (dodecahedra with no hexagons) would not be large enough to accommodate such a core at all; perhaps this is one reason why they never form.] Alternatively, core size is expressed as the diameter of a solid mass of terminal domains, as if they all collapsed together to form the internal "nuggets" seen after negative staining (cf. Fig. 25).

technique, may be quite different from its configuration in suspension. Moreover, the struts and vertices in deep-etched clathrin baskets look completely smooth, with no hint of how the trimers are packed within them. The images provided here do, however, add useful data regarding the relative dimensions of the protomer versus the polymer.

Proximal Arm Length Versus Polygon Edge Length

Measurements of coated pits *in situ,* coated vesicles *in vitro,* and individual basket fragments on mica all indicate that the strut length ($\mathcal{S}$) of an individual polygon (measured vertex to vertex) averages 15.5 nm after freeze etching. This differs significantly from the currently accepted value of 18.5 nm (4, 10, 21, 25, 27), a value which apparently originated with Crowther and Pearse's negative-stain study of basket fragments (1). However, for the reasons outlined in Section 5 of Results, above, we conclude that values of $\mathcal{S}$ greater than 15.5 nm are incorrect, possibly due to incorrect microscope calibration. We belabor this point

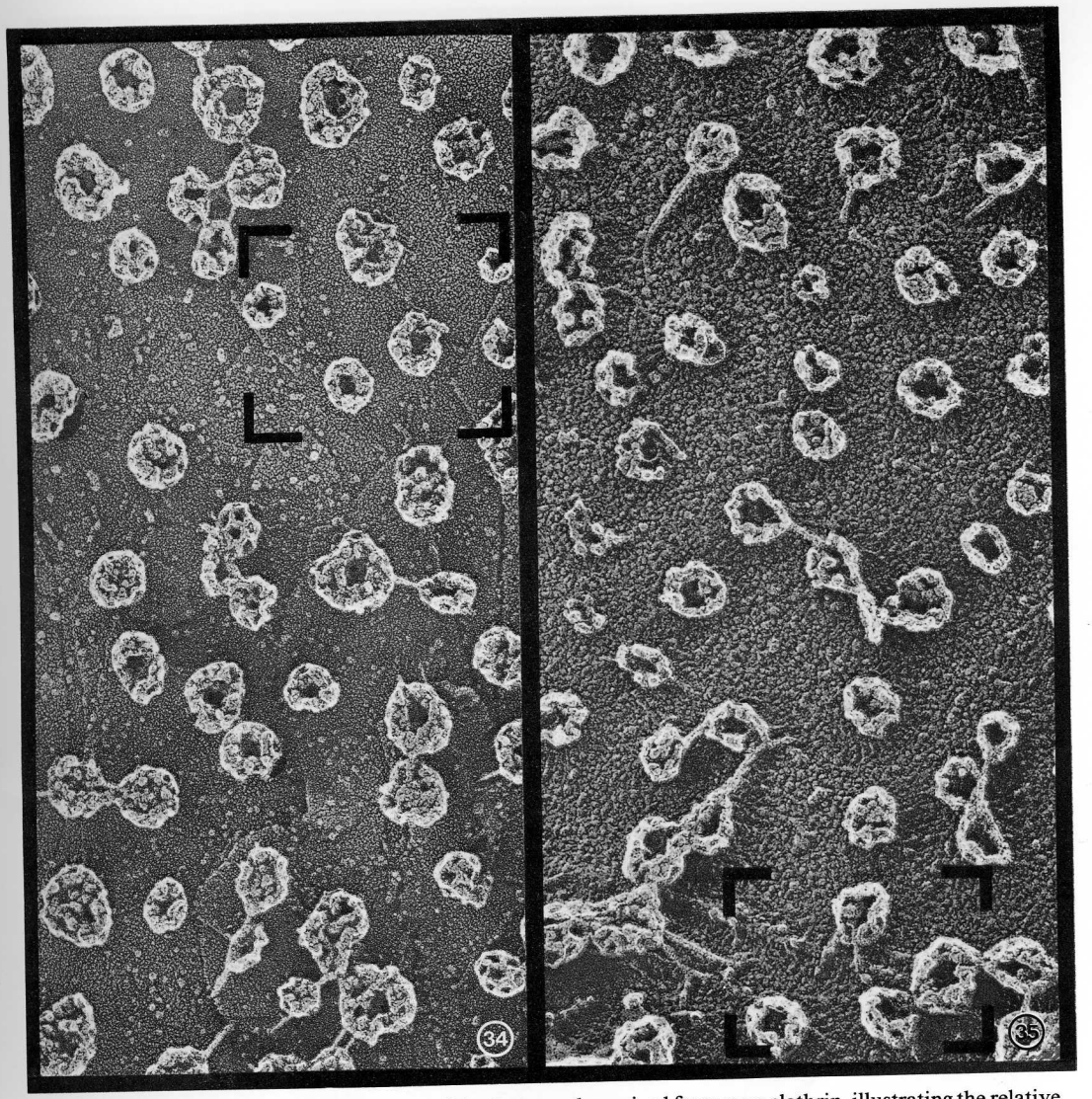

FIGS. 34 AND 35. Freeze fracture of "empty" baskets repolymerized from pure clathrin, illustrating the relative thickness of their walls and narrowness of their internal cavities (Fig. 34), compared with the "clipped" baskets shown in Fig. 35. The bracketed portions of these fields are shown in 3-D in Figs. 36 and 37. Both fields × 105 000.

because the value of $\mathcal{S}$ determines one's choice of packing arrangement of trimers in the completed basket, as described next.

How Triskelions Fit into the Final Polygonal Network

Crowther and Pearse concluded from their observations on negatively stained trimers and basket fragments that the pattern of clathrin arm interdigitation at each vertex is probably that shown in Fig. 38. Central in their thinking was the fact that the struts in completed baskets looked slewed in their negatively stained preparations. However, we have never observed such slew in any type of deep-etched preparation, even though it would be easy to discern, for example, in the broad, flat, purely hexagonal patches of clathrin that abound in cultured fibroblasts (6, 21). We suspect that the neg-

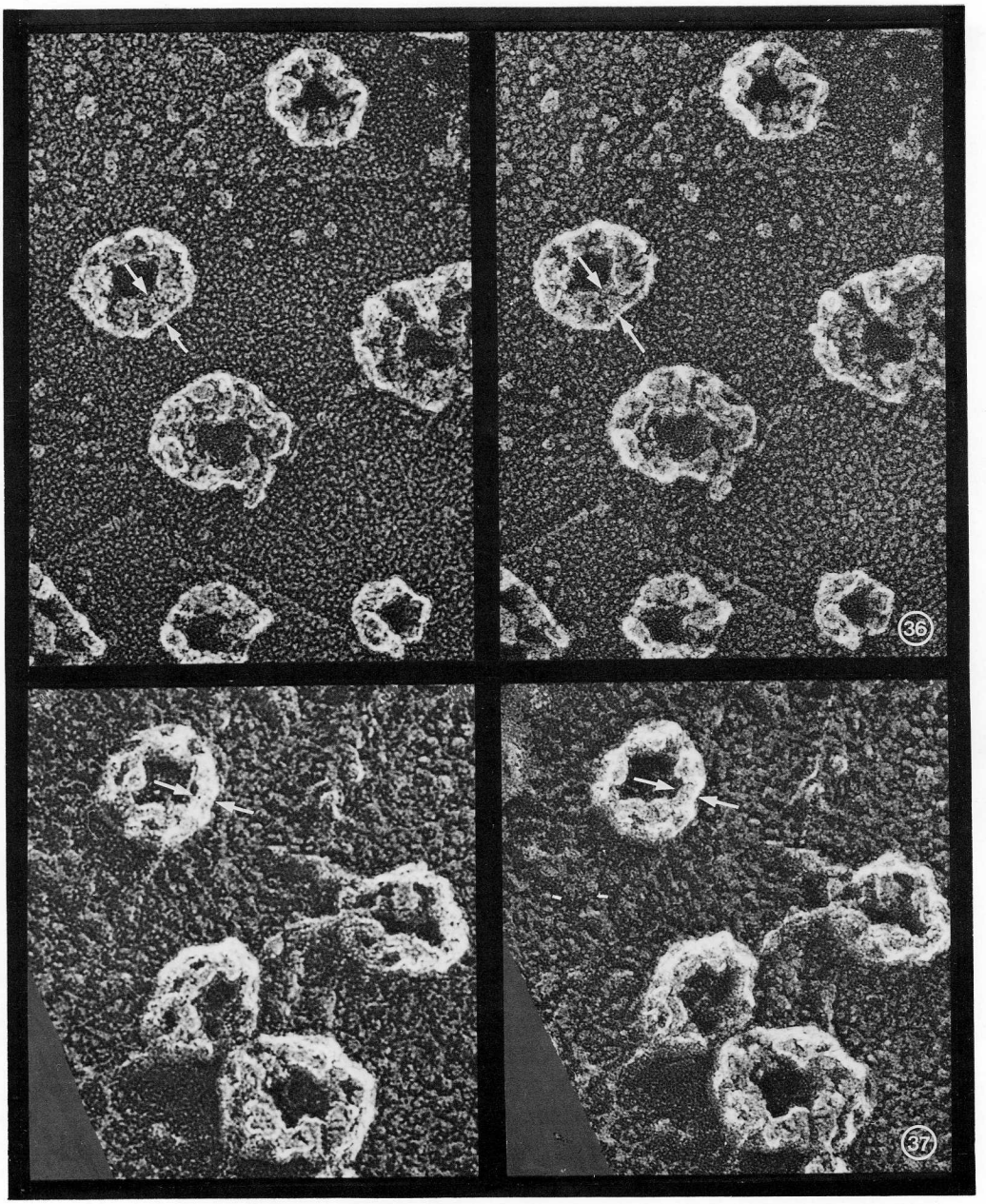

FIGS. 36 AND 37. Stereoscopic views of the bracketed areas in Figs. 34 and 35, illustrating the relative thinness of clipped baskets' walls (cf. opposed arrowheads) which are reduced from ~15 nm normally (in Fig. 36) to ~8 nm after proteolysis (Fig. 37). A thickness of only 8 nm is equivalent to the width of the polygonal struts, implying that inward extensions of the trimer arms have been totally removed. Both fields × 250 000.

atively stained samples in question may have been subjected to some sort of shear before viewing. Moreover, deep-etched clathrin assemblies display no hint of any lateral expansions at the vertices, though these were also predicted by the Crowther and Pearse model. [We acknowledge that in negative stain and thin section images, the peripheral

vertices of clathrin coats have always appeared as "coronas" of relatively large "balls" (2, 5, 9, 19, 23, 32), but we believe this is an artifact of image-overlap and foreshortening of the peripheral vertices as was explained in Ref. (9). Vertices seen *en face* in deep-etch replicas never show any such expansions.]

We are thus required to seek a model of clathrin arm packing that will generate polygons composed of struts that run straight into the vertices, without any expansion of the struts at the vertices. One way to do this would be to bring the arm-bends in, directly beneath each vertex (Fig. 40). However, to do this without disobeying symmetry constraints, we would need to imagine that the origin of each arm at the vertex of a triskelion was displaced in the manner shown for the central (stippled) trimer in Fig. 40 (and shown more clearly in Fig. 43).

A further determinant of the final pattern of clathrin packing in all such models is the exact location of the arm-bends vis-a-vis the final polygonal vertices. [Remember that in all models that envision one clathrin trimer at each vertex, the struts will be composed of four overlapping arm segments: two anti-parallel proximal segments from trimers at immediately adjacent vertices, and two anti-parallel distal segments from two non-adjacent vertices. Symmetry requirements would place the two proximal segments in the same relative positions in the strut, presumably close to the outside, since light chains have been shown to bind to the proximal segments of the trimer arm and to face outwards from the final basket (13, 28, 29, 31).] The question thus boils down to whether the proximal segment of each trimer arm bends *before or after* it reaches the adjacent vertex. Crowther and Pearse concluded that the first bend in their negatively stained trimers was at 16 ± 1 nm, substantially *less* than their estimates of *in situ* strut length $\mathcal{S}$, so they modeled the trimer arm as bending before it reached the next vertex (Fig. 38). More recent measurements place the first bend at ~17 nm from

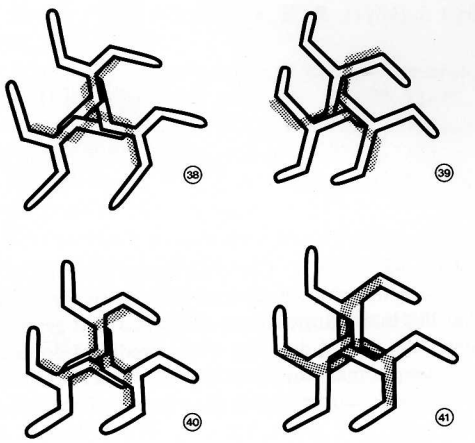

FIGS. 38–41. Four possible patterns of clathrin arm-overlap at a vertex of an assembled basket. Crowther and Pearse's "slewed" packed arrangement [redrawn as a mirror image of their drawing in Ref. (1), to fit with the *external* views of baskets provided by deep-etching] (Fig. 38). The authors of this model originally drew it with clathrin arms infinitely thin, so vertices did not look particularly fat and the proximal portion of each arm appeared to span ~85% of the first polygonal edge before it bent. Since individual clathrin arms are, in fact, half as broad as the whole polygonal strut, this model would actually predict very broad vertices (drawn more precisely in Fig. 42) and proximal arms that extend along only ~65% of the first edge before they bend. As discussed in the text, this does not fit with current estimates of the distance to the first bend in isolated triskelions (~17 nm) which is >110% of the polygonal edge length $\mathcal{S}$. A variation of the above model in which triskelion arms do not bend until they are beyond the vertices (Fig. 39). This would require that the proximal portions of trimer arms be 35% longer than the length of an edge ($\mathcal{S}$), which would not be inconsistent with actual measurements of protomers vs polymers, but would require that the slew on each strut be opposite in handedness to that predicted in Ref. (1). Our preferred model in which baskets would display tighter-packed vertices and their struts would not slew into the vertices (Fig. 40). Here, proximal arms would bend immediately beneath the vertices and hence would extend along ~80% of the edge ($\mathcal{S}$), a proportion closer to observed values than the 65% of Fig. 38. Also, the vertices would look much more like they actually do in deep-etched baskets. A prediction (Fig. 41) bearing the relation to Fig. 40 that Fig. 39 bears to Fig. 38, namely, longer proximal arms [110% of edge length ($\mathcal{S}$), matching deep-etch values most closely]. This model differs from the above three in predicting an intricate interdigitation of the arms at each vertex. Although this design is geometrically attractive, it might be hard to assemble. Thus at the moment we favor the model in Fig. 40.

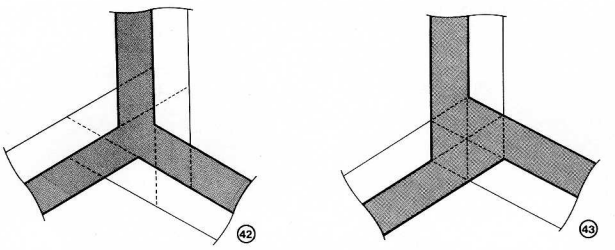

FIGS. 42 AND 43. Correctly scaled drawing of the predicted appearance of a vertex in a clathrin basket, assuming that the slewed-strut packing arrangement proposed by Crowther and Pearse in Ref. (1) is correct (cf. Fig. 38), but taking account of the fact that arms are not as thin as were diagrammed in their report (Fig. 42). Identically scaled drawing of the predicted appearance of the vertex in our preferred model (Fig. 40), where symmetry is maintained by assuming that the individual arms in each clathrin triskelion emanate from its center in a slewed manner, rather than that the final polygonal strut is slewed relative to the center of the vertex (Fig. 43).

the vertex (13–15, 29). Thus proximal arm-length would appear to be substantially *longer* than our new estimate of *in situ* edge-length ($\mathcal{S} \cong 15.5$ nm), not shorter. However, if we attempt to modify Crowther and Pearse's model to take account of this, by making the arms bend *after* they reach the adjacent vertices (Fig. 39), we find that it inverts the slew of the struts and creates the mirror image of what those authors actually saw, thus creating even greater problems for their model. On the other hand, our model in Fig. 40 also fails to satisfy the requirement that the distance to the first bend be longer than $\mathcal{S}$. It too needs to be altered to that in Fig. 41, where the bend occurs after the vertex. This would create a remarkable interdigitation of adjacent trimer arms, undoubtedly stable but possibly hard to assemble initially.

Regardless of which of the models is closer to the truth, both reflect our conviction that the *trimer itself* should slew at its vertex in the manner shown in Fig. 43. In other words, we envision that the individual trimer would adsorb the vertex-asymmetry inherent in any of the triple-crossover models of clathrin packing, rather than the entire lattice would end up slewed. This is the only way we can explain the total *absence* of slew observed in our deep-etch replicas.

We have looked hard for individual slewed-vertex trimers, but have found no clear-cut examples as yet. ("triskelial" trimers adsorbed from Tris are particularly disappointing in this respect; their vertices are so elevated and so coated with platinum that the angle of emergence of their arms is undiscernible.) Further efforts to look for this feature seem warranted.

This work was supported by USPHS grants to J.H., NS-17757 and GM-29647. Special thanks to Robyn Roth for preparing all the replicas, Lori Van Houten and Comfree Coleman for preparing the final plates, and Jan Wuelling for the typing.

REFERENCES

1. CROWTHER, R. A., AND PEARSE, B. M. F. (1981) *J. Cell Biol.* **91,** 790–797.
2. CROWTHER, R. A., FINCH, J. T., AND PEARSE, B. M. F. (1976) *J. Mol. Biol.* **103,** 785–798.
3. FINE, R. E., AND OCKLEFORD, C. D. (1984) *Int. Rev. Cytol.* **91,** 1–43.
4. HARRISON, S. C., AND KIRCHHAUSEN, T. (1983) *Cell* **33,** 650–652.
5. HEUSER, J. E., AND REESE, T. S. (1977) *in* E. R. KANDEL (Ed), Handbook of Physiology, Section I: The Nervous System, Vol. 1, Am. Physiol. Soc., Bethesda.
6. HEUSER, J. (1980) *J. Cell Biol.* **84,** 560–583.
7. HEUSER, J. E. (1981) *Cell* **22,** 634–636.
8. HEUSER, J. E. (1983) *J. Mol. Biol.* **169,** 155–195.
9. KANASEKI, T., AND KADOTA, K. (1969) *J. Cell Biol.* **42,** 202–220.
10. KEEN, J. H. (1985) *in* I. H. PASTAN AND M. D. WILLINGHAM (Eds.), Receptor Mediated Endocytosis, Plenum, N.Y.
11. KEEN, J. H., WILLINGHAM, M. C., AND PASTAN, I. H. (1979) *Cell* **16,** 303–312.

12. KIRCHHAUSEN, T., AND HARRISON, S. C. (1981) *Cell* **23,** 755–761.
13. KIRCHHAUSEN, T., HARRISON, S. C., PARHAM, P., AND BRODSKY, F. M. (1983) *Proc. Natl. Acad. Sci. USA* **80,** 2481–2485.
14. KIRCHHAUSEN, T., AND HARRISON, S. C. (1984) *J. Cell Biol.* **99,** 1725–1734.
15. KIRCHHAUSEN, T., AND HEUSER, J. E. (1984) *J. Cell Biol.* **99,** 366a.
16. KLUG, A., AND FINCH, J. T. (1965) *J. Mol. Biol.* **11,** 403–423.
17. LISANTI, M. P., SCHOOK, W., MOSKOWITZ, N., BECKENSTEIN, K., BLOOM, W. S., ORES, C., AND PUSZKIN, S. (1982) *Eur. J. Biochem.* **121,** 617–622.
18. NANDI, P. K., PRETORIUS, H. T., LIPPOLDT, R. E., JOHNSON, M. L., AND EDELHOCH, H. (1980) *Biochemistry* **19,** 5917–5921.
19. PEARSE, B. M. F. (1975) *J. Mol. Biol.* **97,** 93–98.
20. PEARSE, B. M. F. (1976) *Proc. Natl. Acad. Sci. USA* **73,** 1255–1259.
21. PEARSE, B. M. F. (1980) *Trends Biochem. Sci.* **5,** 131–134.
22. PEARSE, B. M. F., AND ROBINSON, M. S. (1984) *EMBO J.* **3,** 1951–1957.
23. ROTH, T. F., AND PORTER, K. R. (1964) *J. Cell Biol.* **20,** 313–332.
24. SCHMID, S. C., MATSUMOTO, A. K., AND ROTHMAN, J. E. (1982) *Proc. Natl. Acad. Sci. USA* **79,** 91–95.
25. STEVEN, A. C., HAINFELD, J.F., WALL, J. S., AND STEER, C. J. (1983) *J. Cell Biol.* **97,** 1714–1723.
26. UNGEWICKELL, E., AND BRANTON, D. (1981) *Nature (London)* **289,** 420–422.
27. UNGEWICKELL, E., AND BRANTON, D. (1982) *Trends Biochem. Sci.* **7,** 358–361.
28. UNGEWICKELL, E., UNANUE, E., AND BRANTON, D. (1982) *Cold Spring Harbor. Symp. Quant. Biol.* **57,** 723–731.
29. UNGEWICKELL, E. (1983) *EMBO J.* **2,** 1401–1408.
30. VAN JAARSVELD, P. P., NANDI, P. K., LIPPOLDT, R. E., SAROFF, H., AND EDELHOCH, H. (1981) *Biochemistry* **20,** 4129–4135.
31. WINKLER, F. K., AND STANLEY, K. K. (1983) *EMBO J.* **2,** 1393–1400.
32. WOODWARD, M. P., AND ROTH, T. F. (1979) *J. Supramol. Struct.* **11,** 237–250.
33. ZAREMBA, S., AND KEEN, J. H. (1983) *J. Cell Biol.* **97,** 1339–1347.